Spring 2019

Development of Cardanol-based Epoxy Coating

Nicholas Pottschmidt
nsp16@zips.uakron.edu

Development of Cardanol-based Epoxy Coating

Nicholas Pottschmidt

Department of Chemical and Biomolecular Engineering

Honors Research Project

Submitted to

The University of Akron Williams Honors College

Academic Supervisors: Dr. Qixin Zhou and Haoran Wang

Development of Cardanol-based Epoxy Coating

Nicholas Pottschmidt

Department of Chemical and Biomolecular Engineering

Honors Research Project

Submitted to

The University of Akron Williams Honors College

Approved:	**Accepted:**
_____ **Date** _____	_____ **Date** _____
Honors Project Sponsor (signed)	**Department Head (signed)**
_____	_____
Honors Project Sponsor (printed)	**Department Head (printed)**
_____ **Date** _____	_____ **Date** _____
Reader (signed)	**Honors Faculty Advisor (signed)**
_____	_____
Reader (printed)	**Honors Faculty Advisor (printed)**
_____ **Date** _____	_____ **Date** _____
Reader (signed)	**Dean, Honors College**
_____	
Reader (printed)	

Table of Contents

Abstract

The purpose of this project was to determine the suitability of cardanol glycidyl ether (CGE) as a substitute for trimethylolpropane triglycidyl ether (TMPGE) as the reactive diluent in epoxy coatings. CGE may be a naturally-derived alternative to TMPGE, which is a commonly-used petroleum-derived reactive diluent. Epoxy coatings were formulated with CGE replacing increasing amounts of TMPGE in the formulation. Corrosion protection provided by the coatings was evaluated with electrochemical impedance spectroscopy (EIS). Mechanical properties of the coatings (hardness, flexibility, adhesion, and impact resistance) were evaluated with applicable ASTM standards.

EIS results revealed the coating formulated with only CGE had superior corrosion protection when compared to the control formulated with only TMPGE. The control exhibited greater hardness when compared to the coating formulated with only CGE. No measurable differences could be determined within the scopes of the flexibility, adhesion, and impact resistance tests. The results suggest that CGE may be a suitable substitute for TMPGE in epoxy coatings, especially if very good corrosion protection is desired.

1 Executive Summary

Epoxy coatings are commonly used to combat corrosion of metal structures. Many components in epoxy coatings are derived from petroleum compounds. Due to increasing petroleum prices and increasing government regulations applied to petroleum products, it may be beneficial to replace petroleum-derived epoxy coating components with bio-based alternatives. One possible component where this substitution could be made is the reactive diluent. Reactive diluents are incorporated into epoxy coating formulations to decrease the amount of volatile organic compounds and to increase crosslinking between other components of the epoxy formulation. Trimethylolpropane triglycidyl ether (TMPGE), a petroleum derivative, is often used as a reactive diluent. This study focused on replacing TMPGE with cardanol glycidyl ether (CGE), which is derived from cashew nut shells. Coatings were evaluated to determine how substituting CGE for TMPGE affected coating performance. One coating contained only TMPGE as the reactive diluent (the control), one coating substituted some TMPGE with CGE, one coating substituted most of the TMPGE with CGE, and one coating substituted all of the TMPGE with CGE. Corrosion properties and mechanical properties were analyzed.

Polarization resistance (R_p) was used to evaluate the corrosion protection provided by the coatings. On day 1, the coating formulated with only CGE had an R_p value roughly 5 times that of the control. On day 4, it had an R_p value roughly 12 times that of the control. On day 53, it had an R_p value roughly 25 times that of the control. On day 81, it had an R_p value roughly 30 times that of the control. Coatings with both TMPGE and CGE had R_p values between those of the control and the coating formulated with only CGE. All coatings had tape adhesion test values of 4B or 5B. The control had a pencil test hardness value of 6H. Coatings with both TMPGE and CGE had pencil test hardness values of 5H. The coating formulated with only CGE had a pencil test hardness of 4H. The control, the coating with more TMPGE than CGE, the coating with more CGE than TMPGE, and the coating with only CGE had average pendulum hardness test times of 166.0 s, 149.7 s, 139.0 s, and 103.0 s, respectively. All coatings

had mandrel bend test flexibilities greater than 32% elongation. All coatings had an impact resistance greater than 200 kg cm.

The results suggest that replacing TMPGE with CGE had a positive impact on corrosion protection. They also suggest that replacing TMPGE with CGE had a negative impact on coating hardness. Replacing TMPGE with CGE did not have a measurable effect on coating adhesion, flexibility, or impact resistance within the scope of the tests conducted.

Over the course of this project, I developed several technical skills. I learned how to formulate and apply epoxy coatings. I achieved a greater confidence of operating electrochemical impedance spectroscopy (EIS) testing and became more proficient at analyzing and interpreting EIS data. I also learned how to conduct and interpret mechanical tests that are commonly used to study coatings, including adhesion, hardness, flexibility, and impact resistance tests.

The results of this project could be of benefit to society overall. CGE was identified as a possible substitute for TMPGE. Since CGE is a bio-based component, it could help to reduce the amount of petroleum-derived compounds in epoxy coatings. Additional work could identify other opportunities for bio-based components to replace petroleum-based components.

Future technical work should be pursued regarding the results of this project. Testing was only conducted with the coatings exposed to a 3.5 wt% sodium chloride solution. Conducting testing with the coating exposed to different environments would help to determine the versatility of CGE as a possible reactive diluent. It would also be worthwhile to conduct testing with a zinc-rich pigment formulated into the coating. Zinc is more chemically active than steel (the substrate the coatings were applied to for testing) is, meaning that the zinc would oxidize preferentially to the steel if the coating was scratched and bare steel was exposed. Determining the cost differences involved with substituting CGE for TMPGE would help to determine the economical viability of CGE as a reactive diluent.

2 Introduction

2.1 Introduction to Corrosion

Corrosion is a serious issue in a world dependant on metals. In nature, pure metals are rarely encountered; most metals are found in an oxidized form present in ores. Most metals have a thermodynamic tendency to corrode and revert to the oxide form in which they are naturally encountered. Metals prized for their mechanical properties, such as steels, are susceptible to corrosion if left unprotected. NACE International, the global professional organization for the corrosion control industry, estimates that the global cost of corrosion is roughly $2.5 trillion dollars (roughly 3.4% of the world's GDP in 2013)[1]. As a result, many different corrosion mitigation methods are employed today to maintain the integrity of metal structures.

Corrosion is an electrochemical reaction that requires four components to occur: a site where metal is oxidized (anodic site), a conductive electrolyte in contact with the metal, a site on the metal where species in solution are reduced (cathodic site), and a metallic connection between the anodic and cathodic sites[2]. A simplified illustration of corrosion can be found in **Figure 1** (from Jones[2]). In the illustration, a metal ("M") is exposed to an aqueous hydrochloric acid solution (a conductive electrolyte). At the anodic site near the top of the illustration, metal atoms are oxidized to form metal ions (M^{2+}). Electrons lost by the oxidized metal atoms are carried by the bulk of the metal to the cathodic site (near the bottom of the illustration). At the cathodic site, electrons combine with hydrogen ions (H^{+}) to form hydrogen gas (H_2). As this corrosion process proceeds, the surface of the metal is oxidized and dissolved into the solution. Note that anodic sites and cathodic sites can be present at different locations on the same piece of metal.

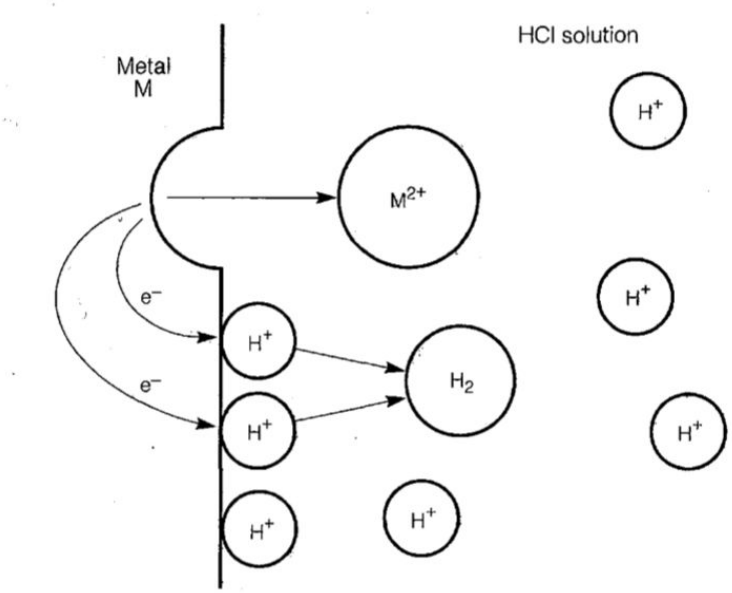

Figure 1: An illustration of the corrosion process when a metal is exposed to an aqueous hydrochloric acid solution[2].

The exact reactions that occur during the corrosion process depend on which metal is being oxidized and which chemical species are present in the metal's environment. Noble metals, like gold and platinum, resist corrosion in all but the most severe of environments. Other metals, like silver or chromium, develop thin films of corrosion products on their surfaces. Once this thin film is formed, corrosion is significantly reduced (this process is referred to as "passivation"). Other metals, like iron and steels, do not undergo passivation and will actively corrode when exposed to the appropriate environment. Chemical species present in the metal's environment may include hydrogen ions and oxygen gas. Oxidizing species like nitrates and sulfates can promote more aggressive corrosion mechanisms depending on the metal.

2.2 Introduction to Protective Coatings

Eliminating any of the four components (anodic site, cathodic site, metallic connection, or electrolyte) from the equation will effectively stop corrosion. One popular method to mitigate corrosion is by using a coating to isolate the electrolyte from the surface of the metal. A wide variety of coatings exists to match the wide variety of situations where corrosion may be an issue. Many factors must be considered when selecting a coating for a corrosion mitigation application. First of all, a coating must be compatible with its service environment to successfully protect a metal structure. Temperature, pH, oxygen content, moisture content, and exposure to ultraviolet radiation (often from sunlight) are all factors that could affect a coating's ability to perform well in its service environment. Secondly, different applications require different service life lengths, ranging from weeks to decades. A coating must perform well for the duration of its service life, regardless of how long its service life may be. Other considerations include how durable the coating must be, how thick the coating must be, and how well the coating adheres to the metal substrate. All of these factors are important to consider to ensure a coating is capable of protecting a metal structure from corrosion.

Other considerations of growing importance go beyond the performance of the coating. The compositions of coatings have become increasingly important in recent years due to government regulations and rising raw material costs. Many coatings are formulated with components derived from petroleum-based products, which are subject to cost increases in the future as petroleum prices rise due to increasing demand and decreasing supply. Government regulations have been affecting petroleum-based compounds (e.g. volatile organic compounds) in the past and likely in the future[3]. Therefore, it is desirable to possibly limit the amount of petroleum-based compounds in protective coatings.

2.3 Introduction to Epoxy Coatings

Epoxy coatings are a type of commonly used coatings to mitigate corrosion. The key building block of an epoxy coating is an epoxy resin. A commonly used epoxy resin is bisphenol A (BPA) epoxy resin. BPA epoxy resin is formed by reacting epichlorohydrin with BPA. **Figure 2** illustrates the molecular structures of epichlorohydrin (from Wicks[4]) and BPA (from Sigma-Aldrich[5]).

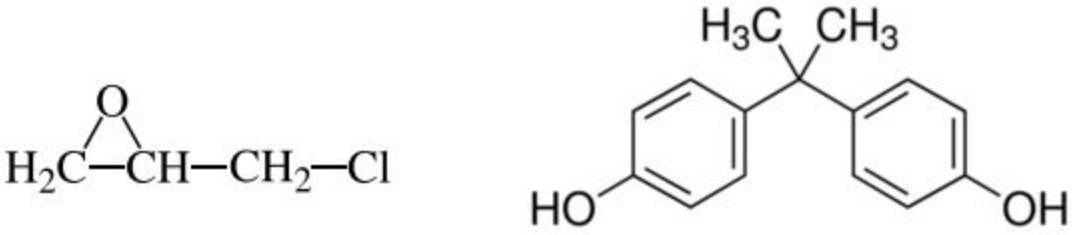

Figure 2: Molecular structures of epichlorohydrin[4] (left) and BPA[5] (right).

The epoxide group and chlorine on the epichlorohydrin react with hydroxyl groups on the BPA to form large BPA epoxy resin molecules. **Figure 3** illustrates the molecular structure of the resulting BPA epoxy resin (from Wicks[4]).

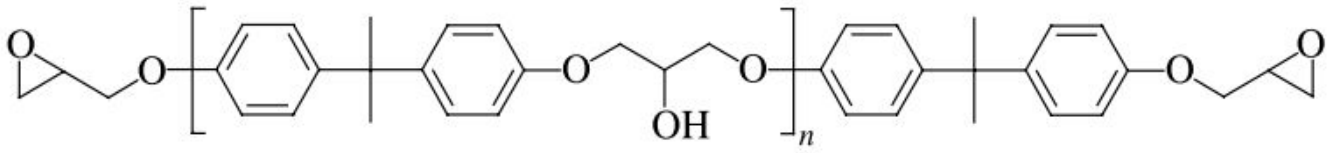

Figure 3: Molecular structure of BPA epoxy resin[4].

To create a durable coating, BPA epoxy resin is reacted with curing agents (also referred to as "crosslinkers") to chemically bond adjacent BPA epoxy resin molecules. For this study, Epikure 3192 (a polyamidoamine produced by Hexion Incorporated) was used to react with the BPA epoxy resin.

A common addition to epoxy coating formulations is a wetting agent. A wetting agent accomplishes what its name suggests- it improves the wetting of a coating on a substrate. Wetting depends on the surface tension of the coating and the surface tension of the substrate to be coated[6]. Wetting occurs if the surface tension of the coating is less than the surface energy of the substrate[6]. If a coating's surface tension is greater than a substrate's surface energy, a wetting agent can be employed to ensure proper wetting.

The last major component of an epoxy coating formulation is the solvent. The solvent acts as the carrier for the other components of the coating and is usually an organic compound. Xylene, a volatile aromatic hydrocarbon, is often used as a solvent for epoxy formulations. A drawback to volatile organic compounds like xylene is that they readily vaporize into the atmosphere. Because of this, volatile organic compounds are regulated to minimize harm to the environment[3].

A common way to reduce volatile organic compound content is by replacing some of the solvent with a reactive diluent. Unlike solvent (which volatilizes after the coating is applied), a reactive diluent reacts with other components in the epoxy formulation to increase crosslinking in the coating. Because of this, reactive diluents are beneficial for two reasons: they reduce volatile organic compound content and help to create a more robust coating upon curing. Trimethylolpropane triglycidyl ether (TMPGE) is a commonly used reactive diluent and is illustrated in **Figure 4** (from Sigma-Aldrich[7]). The three epoxide groups present in TMPGE allow the molecule to crosslink with other components in the epoxy formulation. A major drawback of TMPGE is that it is obtained from petroleum-derived sources. Because of this, bio-based reactive diluent alternatives could be used in epoxy coating formulations to reduce the content of petroleum-derived components.

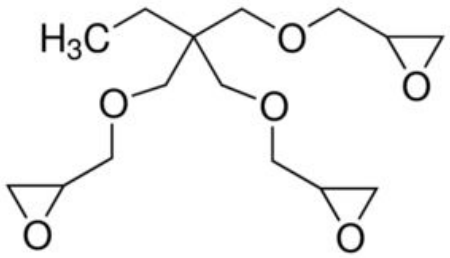

Figure 4: Molecular structure of TMPGE[7].

In this study, cardanol glycidyl ether (CGE) was investigated as a possible substitute for TMPGE as the reactive diluent in epoxy formulations. CGE is derived from cardanol, a substance that is readily obtained from cashew nut shells. **Figure 5** illustrates the molecular structure of CGE.

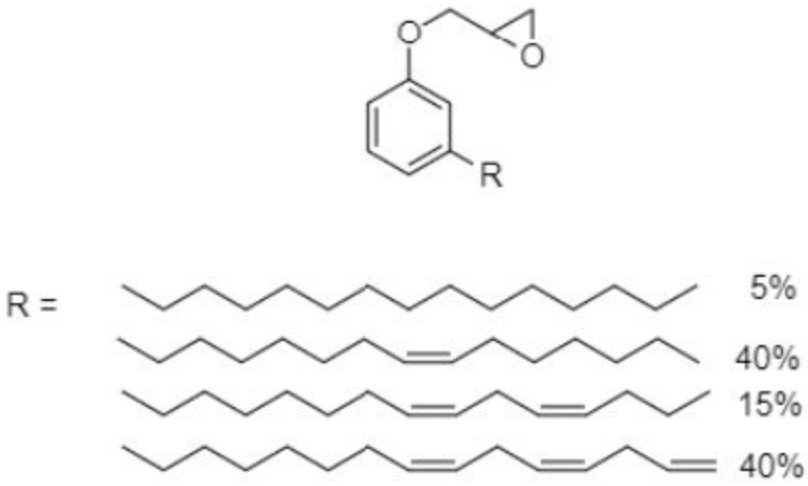

Figure 5: Molecular structure of CGE.

Since CGE is obtained from a renewable, bio-based source, it is an attractive potential alternative to TMPGE. To determine the effectiveness of CGE as a reactive diluent, epoxy coatings must be formulated and tested to determine how their performance compares to that of epoxy coatings formulated with TMPGE. Using cardanol derivatives to replace epoxy components is a continuation of other work aimed at incorporating cardanol derivatives into various types of coating systems[8].

2.4 Epoxy Coating Formulations Tested

In order to test the effectiveness of CGE as a reactive diluent, four different epoxy coatings were formulated with varying amounts of CGE and TMPGE present. The first formulation (E0) was a control with only TMPGE present. In the next two formulations (E10 and E20), varying amounts of both CGE and TMPGE were present. In the fourth formulation (E30), only CGE was present. **Table 1** lists the compositions of the four epoxy coating formulations that were tested. The compositions are listed as weight percents. Note that the weight percents are not uniform for other components across the four formulations. This is because the formulations were calculated based on the activity of important functional groups present on the molecules and not on molecular weight.

Table 1: Epoxy coating formulations investigated in this study. All percentages are determined by weight.

Epoxy Coating Name	BPA Epoxy Resin	Curing Agent	CGE	TMPGE	Xylene	Wetting Agent
E0	37.31%	40.90%	0.00%	15.97%	4.93%	0.90%
E10	38.49%	39.18%	5.47%	11.01%	4.93%	0.92%
E20	39.75%	37.36%	11.37%	5.64%	4.93%	0.95%
E30	41.08%	35.41%	17.58%	0.00%	4.93%	0.99%

2.5 Performance Testing Overview

It is impossible to predict how a coating will perform during its service life with perfect accuracy. However, performance testing conducted in the laboratory can often be used to predict how well a coating will perform relative to other coatings. Both the corrosion mitigation properties and the mechanical properties of the coatings can be tested in the laboratory. All performance testing is conducted on coatings applied to UNS G10080 cold rolled steel test panels. Corrosion protection is evaluated with

electrochemical impedance spectroscopy (EIS). Mechanical testing involves evaluating the coatings' adhesion to the test panels (ASTM D3359[9]), the coatings' hardness (ASTM D4366[10] and ASTM D3363[11]), and the coatings' flexibility (ASTM D522[12]). Impact resistance is also tested to determine how the coatings react to sudden impacts. The performances of epoxy coatings made from the petroleum-based reactive diluent and the cardanol-based reactive diluent are compared. The results can help to determine whether or not CGE may be a suitable substitute for TMPGE in the epoxy coatings that were tested.

3 Background

3.1 Electrochemical Impedance Spectroscopy

Various electrochemical tests can be used to measure the corrosion rate of a coated steel sample. EIS is particularly useful, because its use of alternating current can be used to predict the corrosion mechanism in addition to measuring the corrosion rate. Since corrosion is an electrochemical process, it can be reasonably be modeled as an electrical circuit composed of resistors and capacitors. Resistors impede the flow of electrical current and capacitors store electrical energy in electric fields. Sources of resistance that may be present in corrosion circuits include resistance caused by the electrolyte solution (R_s), resistance caused by the coating (R_{coat}), resistance caused by pores (defects) that may be present in the coating (R_{pore}), and polarization resistance caused by charge transfer at the metal/electrolyte interface (R_p). Capacitors that may be present in corrosion circuits include capacitance caused by the coating (C_{coat}) and capacitance present at the metal/electrolyte interface (C_{dl}).

An electrochemical double layer exists at the metal/electrolyte interface. As corrosion proceeds, gases may evolve at the interface and reactants may become depleted at the interface. Gas evolution and reactant depletion cause an electrochemical double layer to form at the interface that behaves both as a resistor (R_p) and as a capacitor (C_{dl}).

There are several commonly encountered equivalent electrical circuits used to model corrosion processes. The first equivalent circuit models actively corroding bare metal. In this model, there is both polarization resistance (R_p) and electrochemical double layer capacitance (C_{dl}) due to interactions at the metal/electrolyte interface. Solution resistance (R_s) caused by interactions in the electrolyte is also present. **Figure 6** illustrates the equivalent circuit for an actively corroding piece of metal.

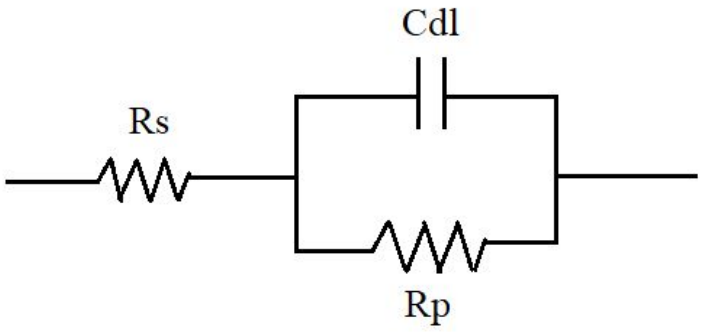

Figure 6: Equivalent circuit for actively corroding bare metal. R_s corresponds solution resistance and C_{dl} and R_p represent interactions at the metal/electrolyte interface.

The second commonly encountered equivalent circuit models metal protected by a perfect coating. In reality, no coating is truly perfect, but this equivalent circuit is a reasonable approximation for intact coatings. This equivalent circuit is similar to that of actively corroding bare metal. In this model, there is both coating resistance (R_{coat}) and coating capacitance (C_{coat}) due to interactions at the coating/electrolyte interface. Solution resistance (R_s) caused by interactions in the electrolyte is also present. Since the metal is not directly exposed to the electrolyte, R_p and C_{dl} are excluded from this model. **Figure 7** illustrates the equivalent circuit for metal protected by a theoretically perfect coating.

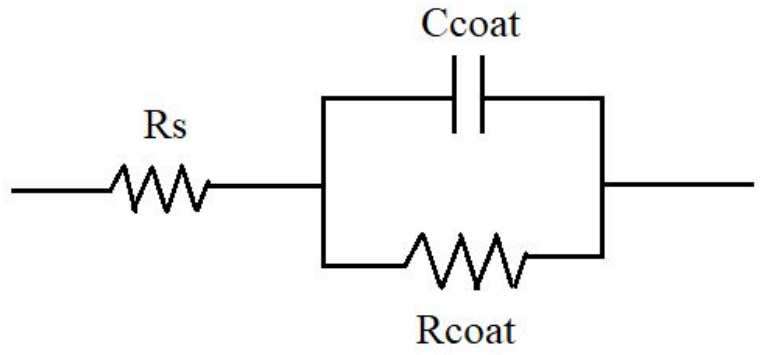

Figure 7: Equivalent circuit for metal protected by a perfect coating. R_s corresponds solution resistance and C_{coat} and R_{coat} represent interactions at the coating/electrolyte interface.

The third commonly encountered equivalent circuit takes into account the presence of defects on a coated metal sample. This model is especially useful when a coating has defects or begins to break down due to extended exposure to a corrosive environment. As is the case for the previous two models, solution resistance (R_s) is present. Coating capacitance (C_{coat}) is present to model the capacitance of the coating regions that are still intact. A new parameter is introduced to represent resistance caused by the presence of pores (defects) in the coating (R_{pore}). Polarization resistance (R_p) and double layer capacitance (C_{dl}) are present in this model to represent the metal/electrolyte interface in the pores. **Figure 8** illustrates the equivalent circuit for metal protected by a imperfect (defective) coating.

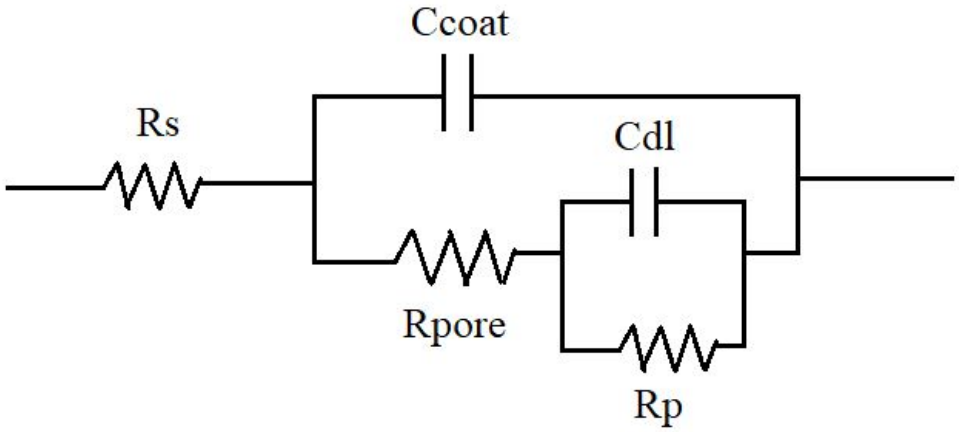

Figure 8: Equivalent circuit for metal protected by a defective coating. R_s corresponds solution resistance, C_{coat} represents capacitance of the coating, R_{pore} represents resistance of the defects, R_p represents polarization resistance, and C_{dl} represents double layer capacitance.

The interfaces modeled by capacitors in the previous equivalent circuits do not always behave as ideal capacitors. This discrepancy is dealt with by using constant phase elements (CPEs) in place of capacitors in the circuits. The nature of what a CPE actually is is not known[13], but it is useful for determining more accurate values of R_p, R_{pore}, and R_s. The following is the equation **(Equation 1)** for the impedance of a CPE:

$$Z_{CPE} = \frac{1}{(j\omega)^a Q} \quad \textbf{(1)}$$

Where j is the unit imaginary number, ω is the frequency of the alternating current, a is an exponential factor, and Q is the capacitance associated with the CPE. For comparison, the following is the equation **(Equation 2)** for the impedance of a perfect capacitor:

$$Z_C = \frac{1}{j\omega C} \quad \textbf{(2)}$$

Where C is the capacitance. **Figures 9 and 10** show modified versions of the circuits presented in **Figures 7 and 8** with capacitors substituted with CPEs.

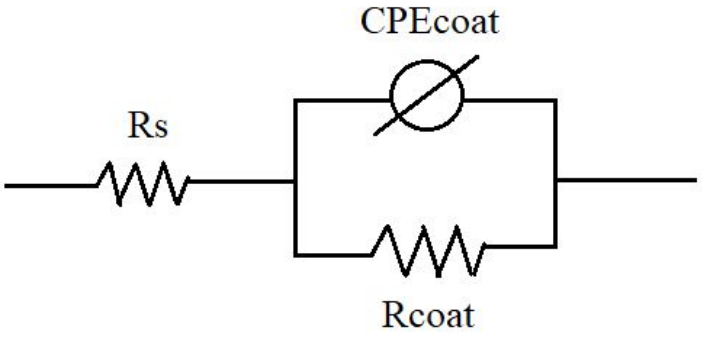

Figure 9: The circuit represented in **Figure 7** with the capacitor substituted with a CPE.

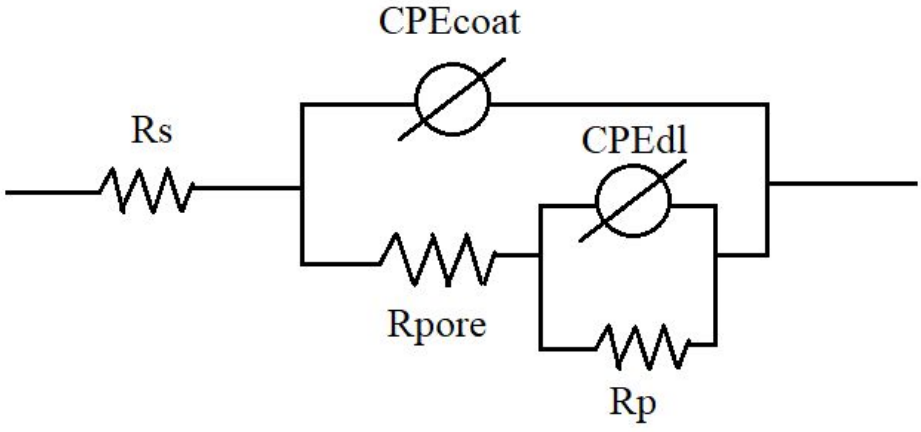

Figure 10: The circuit represented in **Figure 8** with the capacitors substituted with CPEs.

Data from EIS tests can be presented in two types of plots: Nyquist plots and Bode plots. Nyquist plots plot the imaginary component of the electrochemical impedance versus the real component of the electrochemical impedance. Nyquist plots tend to have a semicircle-like appearance. Bode plots plot the magnitude of the electrochemical impedance versus the frequency of the alternating current applied during the EIS test. On Bode plots, magnitude tends to decrease as frequency increases. Different regions on the Nyquist and Bode plots correspond to the parameters present in the circuits illustrated in **Figures 6-10.** Electrochemistry fitting software (such as Gamry Echem Analyst[14]) can be used to fit data to the equivalent circuit models to determine the values of the parameters present in the circuits. **Figures 11 and 12** depict illustrations of generic Nyquist and Bode plots (respectively) for actively corroding metal. These plots correspond to the circuit presented in **Figure 6.** In **Figure 11,** the maximum point on the Nyquist plot represents double layer capacitance (C_{dl}). The leftmost point corresponds to electrolyte solution resistance (R_s), and the difference between the leftmost point and rightmost point corresponds to polarization resistance (R_p). In **Figure 12,** the magnitude of the modulus (Z) on the right side of the Bode plot (higher frequency) corresponds to R_s. The magnitude of the modulus (Z) on the left side of the Bode plot (lower frequency) corresponds to $R_p + R_s$.

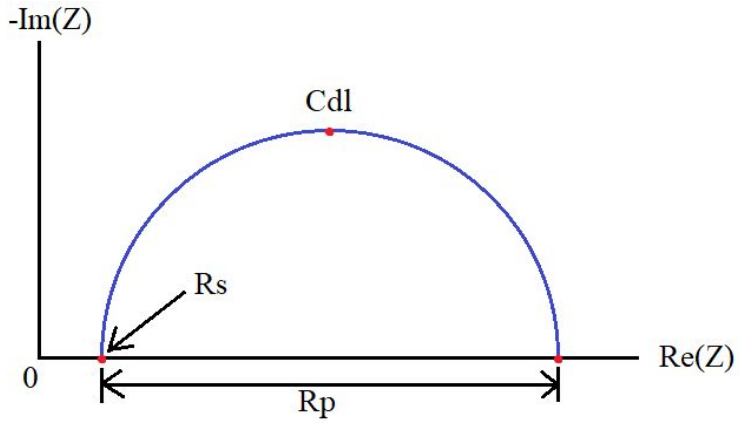

Figure 11: Generic Nyquist plot for actively corroding metal. Important parameters R_s, R_p, and C_{dl} can be obtained from the plot.

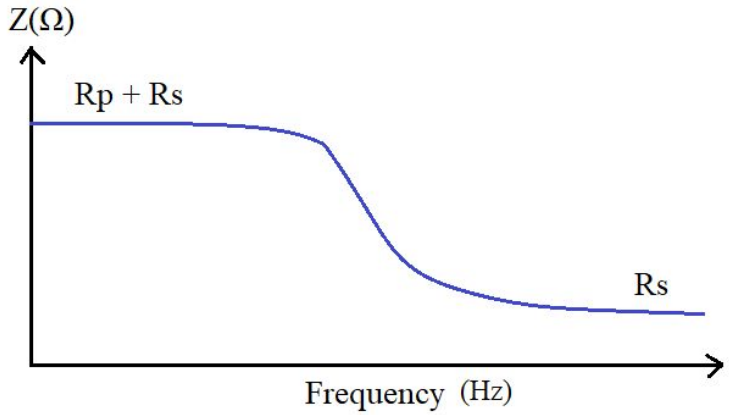

Figure 12: Generic Bode plot for actively corroding metal. Important parameters R_s and R_p can be obtained from the plot.

Figures 13 and 14 depict illustrations of generic Nyquist and Bode plots (respectively) for metal protected by a perfectly intact coating. These plots correspond to the circuit presented in **Figure 7.** As mentioned previously, a perfect coating is more of a theoretical concept than it is an achievable goal, though it is still a reasonable approximation for intact coatings. In **Figure 13,** the maximum point on the Nyquist plot represents coating capacitance (C_{coat}). The leftmost point corresponds to electrolyte solution resistance (R_s), and the difference between the leftmost point and rightmost point corresponds to coating resistance (R_{coat}). In **Figure 14,** the magnitude of the modulus (Z) on the right side of the Bode plot (higher frequency) corresponds to R_s. The magnitude of the modulus (Z) on the left side of the Bode plot (lower frequency) corresponds to $R_{coat} + R_s$.

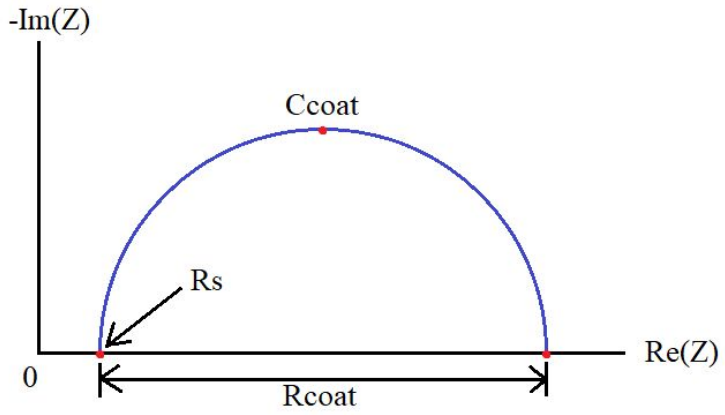

Figure 13: Generic Nyquist plot for metal protected by a perfectly intact coating. Important parameters R_s, R_{coat}, and C_{coat} can be obtained from the plot.

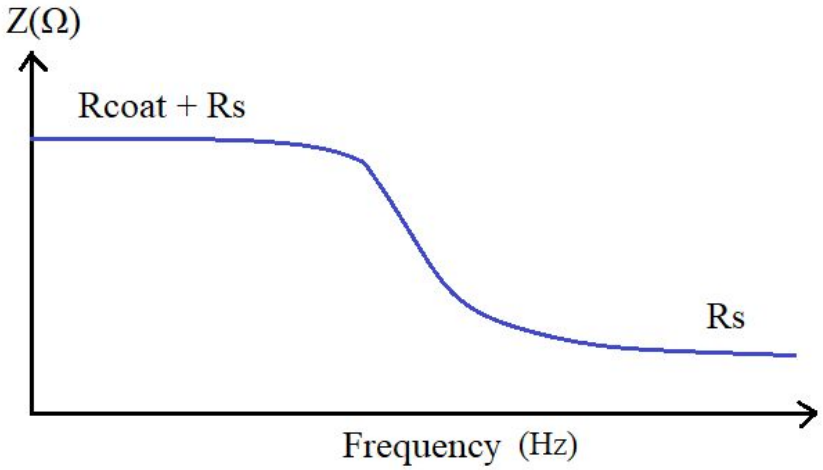

Figure 14: Generic Bode plot for metal protected by a perfectly intact coating. Important parameters R_s and R_{coat} can be obtained from the plot.

Figures 15 and 16 depict illustrations of generic Nyquist and Bode plots (respectively) for metal protected by an imperfect (damaged) coating. These plots correspond to the circuit presented in **Figure 8.** Since coatings can develop defects over time, this model is often best to simulate defective coatings. Both the Nyquist and Bode plots develop a different appearance when coating defects are present. The Nyquist

plot develops an additional semicircle "hump" and the Bode plot develops an additional "plateau." In **Figure 15,** the maximum point on the left "hump" of the Nyquist plot represents coating capacitance (C_{coat}). The maximum point on the right "hump" represents the double layer capacitance (C_{dl}). As with the previous two models, the leftmost point corresponds to electrolyte solution resistance (R_s). The difference between the leftmost point and center minimum point corresponds to pore resistance (R_{pore}). The difference between the center minimum point and the rightmost point corresponds to polarization resistance (R_p). In **Figure 16,** the magnitude of the modulus (Z) on the right side of the Bode plot (higher frequency) corresponds to R_s. The magnitude of the modulus (Z) at the center "plateau" of the Bode plot (middling frequency) corresponds to $R_{pore} + R_s$. The magnitude of the modulus (Z) on the left side of the Bode plot (lower frequency) corresponds to $R_p + R_{pore} + R_s$. Not every Nyquist plot and Bode plot is as neat as those present in the illustrations, so electrochemistry fitting software is used to determine numerical values for the parameters.

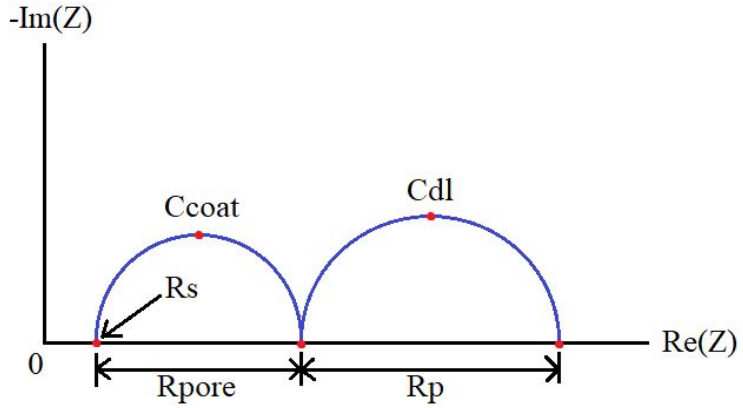

Figure 15: Generic Nyquist plot for metal protected by an imperfect coating. Important parameters R_s, R_{pore}, R_p, C_{dl}, and C_{coat} can be obtained from the plot.

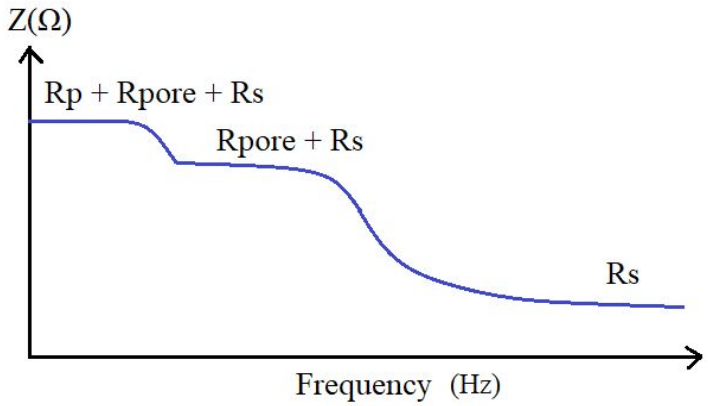

Figure 16: Generic Bode plot for metal protected by an imperfect coating. Important parameters R_s, R_{pore}, and R_p can be obtained from the plot.

Equivalent circuits containing CPEs can obtain essentially the same parameters from Nyquist and Bode plots. The main difference is that fitting softwares extract Q_{coat} and Q_{dl} parameters instead of C_{coat} and C_{dl} parameters.

For corrosion measurement purposes, EIS is most useful because its results can be used to predict corrosion rate. Corrosion rate is directly proportional to corrosion current density (i_{corr}). Corrosion current density is the amount of current associated with the corrosion reaction divided by the surface area of the corroding surface. Corrosion current density is inversely related to polarization resistance (Rp) according to the following equation[2] **(Equation 3)**:

$$i_{corr} = \frac{B}{R_p} \qquad \textbf{(3)}$$

Where B is a parameter related to the corrosion occurring for a given metal in a given environment. Since decreased corrosion rate corresponds to a decrease in i_{corr}, a large R_p valuable corresponds to a low corrosion rate. This means that the larger the R_p value is for a coating, the more effective the coating is at protecting the metal substrate from corrosion. For intact coatings, R_{coat} values can be used in place of R_p values to analyze corrosion rate.

One significant benefit of EIS is that it is a nondestructive test, meaning conducting EIS does not damage a coating and can be conducted multiple times on the same sample. Since coating degradation may require a considerable amount of time to occur, EIS testing is often conducted over a period of many weeks to allow for sufficient time for the coating to break down. Coated samples are continuously exposed to the electrolyte solution over the duration of the multi-week EIS testing period. EIS tests are often ran many times to compare how R_p changes as time goes on. A sudden drop in R_p or the development of a second "hump" on the Nyquist plot often corresponds to the development of a significant defect in the coating.

3.2 Mechanical Property Testing

Several mechanical properties are very important for coatings. These properties include substrate adhesion, hardness, flexibility, and impact resistance. These aspects are important for corrosion performance, since they affect the durability of the coating, which in turn can affect corrosion protection.

A commonly used adhesion test is the tape test (ASTM D3359[9]). Two methods of the tape test are used: Test Method A (for thicker coatings) and Test Method B (for coatings 125 μm (5 mil) or thinner). Since the investigated epoxy coatings were thinner than 125 μm, Test Method B was used. In the tape test, two sets of six cuts are applied to a coated panel with the two sets of cuts perpendicular to each other. Care must be taken to ensure the cuts fully breach the coating. If done correctly, a 5 × 5 grid of squares is applied to the coating. Then, a piece of tape is firmly applied to the 5 × 5 grid (in accordance with ASTM D3359[9]) and is quickly removed. The 5 × 5 grid is closely analyzed to determine if any of the coating was removed by the tape. ASTM D3359[9] provides classifications ranging from 5B (0% of the coating is removed) to 0B (greater than 65% of the coating is removed).

Two commonly used hardness tests are the pencil test (ASTM D3363[11]) and the pendulum hardness test (ASTM D4366[10]). The pencil test is conducted with pencils of various hardnesses ranging

from 6B (softest graphite) to 6H (hardest graphite). Pencils are sharpened with a draftsman-type pencil sharpener and are sanded to ensure the tip of the pencil's graphite is perfectly cylindrical. A wheeled pencil holder is used to drag the pencil across the surface of the coating at a 45° angle. The hardest graphite is tested first, and increasingly softer graphites are used until a hardness is found that does not gouge into the coating. The hardness of the hardest graphite that does not gouge the coating is the coating hardness that is reported for this test.

The König pendulum hardness test (Test Method A in ASTM D4366[10]) is also used to evaluate coating hardness. In the König test, a coated panel is loaded into a König pendulum tester (manufactured by BYK) so that the pendulum pivots in contact with the coating. To begin the test, the pendulum is deflected 6° and released. Once the deflection of the pendulum reaches 3°, the test is stopped and the time to reach 3° deflection is recorded. Increased coating hardness causes longer times to reach 3° deflection. To summarize, longer König pendulum test times correspond to harder coatings.

Coating flexibility is often evaluated with the mandrel bend test (ASTM D522[12]). In this test, a coated cold rolled steel test panel is bent around a mandrel and the coating is carefully analyzed to determine the extent of cracking. ASTM D522[12] describes two different test methods for mandrel bend testing; the conical mandrel test (Test Method A) was used. In the conical mandrel test, a coated test panel is bent around a conical mandrel and examined for coating cracks. The greatest bending and elongation of the coating occurs at the small end of the mandrel, so cracking usually begins there. ASTM D522[12] provides the following chart **(Figure 17)** to estimate the percent elongation experienced by the coating along the mandrel. The greatest elongation of 32% occurs at the small end of the mandrel.

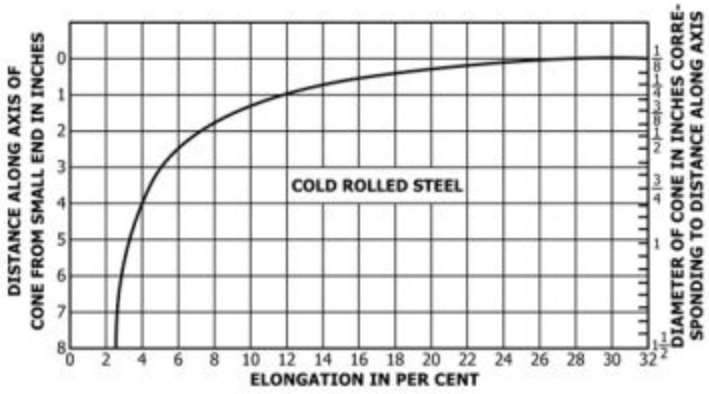

Figure 17: Relationship between position along the mandrel and percent coating elongation. Note that the greatest elongation (32%) occurs at the small end of the mandrel (position 0 in.). Figure is from ASTM D522[12].

The final mechanical test conducted is the impact resistance test. Coatings in real world service environments often sustain sudden impacts from various forms of debris, so it is important for coatings to be able to withstand such impacts. A BYK-Gardner impact tester can be used to drop a 2 kg rounded projectile up to 100 cm on a coated test panel. Impact testing is conducted both with the coated side of the panel in contact with the projectile (forward impact test) and with the uncoated side of the panel in contact with the projectile (reverse impact test). After impact, the coated side of the panel is carefully analyzed to determine if any cracking occurred. If the coating cracked, the test is repeated with the projectile dropped from a lower height. The test is repeated until the highest initial projectile height that does not cause cracking is found. The results of the test are reported as the product of the projectile mass and initial projectile height.

4 Experimental Methods

4.1 Sample Preparation

All laboratory work was conducted with safety in mind. Safety glasses, gloves, and a labcoat were worn when working. When working with hazardous chemicals, a respirator was worn and work was conducted inside of a fume hood to minimize exposure.

The first step of the study involved blending and applying the candidate epoxy coatings onto cold rolled steel test panels. The compositions of the four coatings can be found in **Table 1.** All blending was conducted in small glass vials in batches on the order of 10 g. The following blending procedure was used to prepare the epoxy coatings:

1. Charge BPA resin, CGE (if any), TMPGE (if any), xylene, and wetting agent. Stir on a stir plate until well mixed.
2. Charge curing agent to the batch and allow to mix for 5 minutes.
3. Place batch in sonicator (set to degassing setting) for 5 minutes to force air bubbles out of the batch.
4. Allow batch to stand for 2 minutes.

Since the curing agent was incorporated into the formulation, the epoxy coating had to be applied to a substrate in a timely fashion to prevent the epoxy from solidifying in the glass vial. The selected substrates were QD-36 cold rolled steel test panels manufactured by the Q-Lab Corporation (based in Westlake, Ohio). The QD-36 test panels are made out of UNS G10080 cold rolled steel and have a smooth mill finish. The coatings were applied to the panels with a *drawdown bar*. A drawdown bar is a metal bar with grooves of varying depths (for example, 1 mil, 2 mil, 3 mil or 30 μm, 60 μm, 90 μm). The bar is sat on the test panel with the groove of the desired wet coating thickness touching the test panel. The epoxy is pipetted onto the panel near the groove of the desired wet coating thickness. Then, the bar is carefully dragged along the face of the panel in one continuous motion, leaving a coating of uniform

thickness on the test panel. For this study, the drawdown bar was used to apply coatings with a wet thickness of 90 μm.

After the coatings were applied to the test panels, they were allowed to cure at room temperature (roughly 25 °C) for several hours. Then, the coated panels were placed in an oven at 120 °C for two hours to complete the curing process. After curing in the oven, the coated panels were allowed to cool to room temperature.

4.2 EIS Procedure

To prepare the coated test panels for EIS testing, glass tubes were clamped onto the coating. Rubber gaskets were used between the glass tubes and the coatings to achieve a watertight seal. The gaskets used to prepare samples had a diameter of 19.4 mm, which corresponds to an exposed coating surface area of 2.96 cm^2. Once a watertight seal was achieved, the glass tube was filled most of the way with 3.5 wt% sodium chloride solution. This solution remained in contact with the coating for many weeks. When EIS testing was not actively in progress, the tops of the glass tubes were covered to prevent evaporation of the electrolyte solution.

EIS testing requires three electrodes: a working electrode, a reference electrode, and a counter electrode. For the coatings being tested, the working electrode was the cold rolled steel test panel. A saturated calomel electrode (SCE) was used for the reference electrode. A platinized niobium mesh electrode was used for the counter electrode. All three electrodes were connected to Gamry potentiostats. Care was taken to ensure that none of the electrodes were in contact with each other. Electrodes in contact cause a short in the electrochemical circuit and measurements cannot be taken. Care was taken to ensure that all of the electrodes were in contact with the electrolyte solution. If an electrode is not in contact with the electrolyte, the circuit is open and measurements cannot be taken. During EIS testing, the coated

samples were placed in Faraday cages to reduce electrical interference from equipment present in the laboratory. **Figure 18** is an image of coated test panels connected to potentiostats for EIS testing.

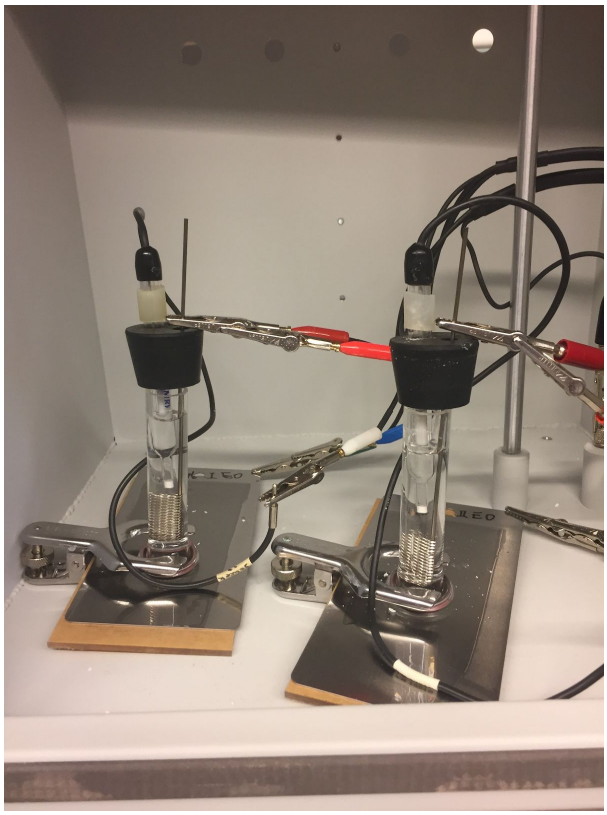

Figure 18: EIS testing setup.

Prior to running the first EIS test for the day, the SCE reference electrodes were allowed to equilibrate in the electrolyte solution for 20 minutes. No additional equilibration was necessary for subsequent EIS tests. An AC voltage of 10 mV was used for EIS testing. The initial AC current frequency was 100000 Hz and the final AC current frequency was 0.01 Hz. EIS testing typically took 20 to 30 minutes per sample to complete. After EIS testing was complete, samples were sealed to prevent evaporation of the electrolyte. SCE reference electrodes and mesh counter electrodes were rinsed with deionized water and dried between EIS tests.

4.3 Mechanical Testing Procedures

The tape adhesion test (ASTM D3359[9]) was conducted with a cutting tool and adhesive tape compliant with the standard. Cuts were carefully applied with the cutting tool to ensure they reached the underlying metal substrate. Two sets of cuts were applied perpendicular to each other to create a 5 × 5 grid of cut coating squares. **Figure 19** displays examples of cut marks on an E10 sample.

After the cuts were applied to the coating, the tape was firmly pressed onto the 5 × 5 grid. The tape was then quickly removed from the coated panel. Care was taken to remove the tape consistently and without forcefully yanking it off of the coated panels. After the tape was removed, the 5 × 5 grid was closely examined with a lit magnifier to determine how much of the coating (if any) was removed by the tape. The coatings were rated according to the classifications listed in Figure 1 in ASTM D3359[9].All testing was conducted by the same operator over the course of an hour to reduce the effects of temperature, humidity, and operator technique on the test results. **Figure 20** displays a magnified 5 × 5 grid after tape was removed from it.

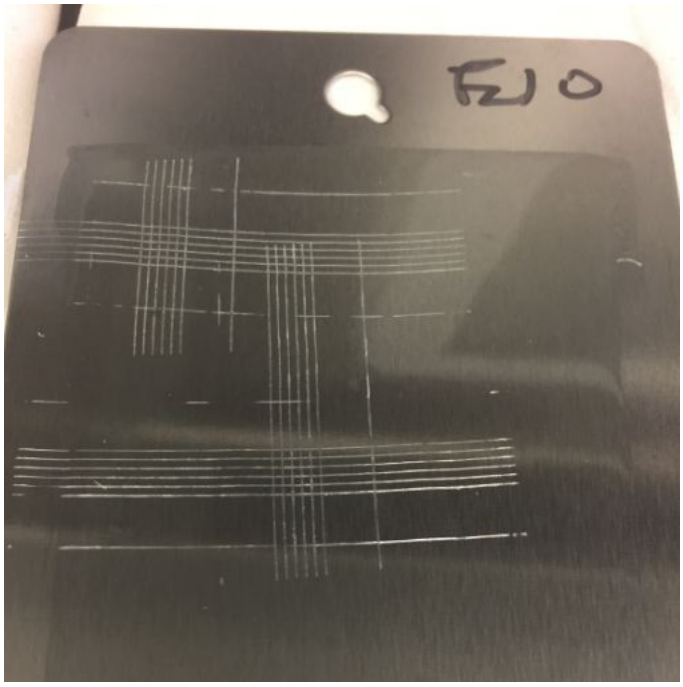

Figure 19: Examples of cut marks inscribed on an E10 sample for tape adhesion test.

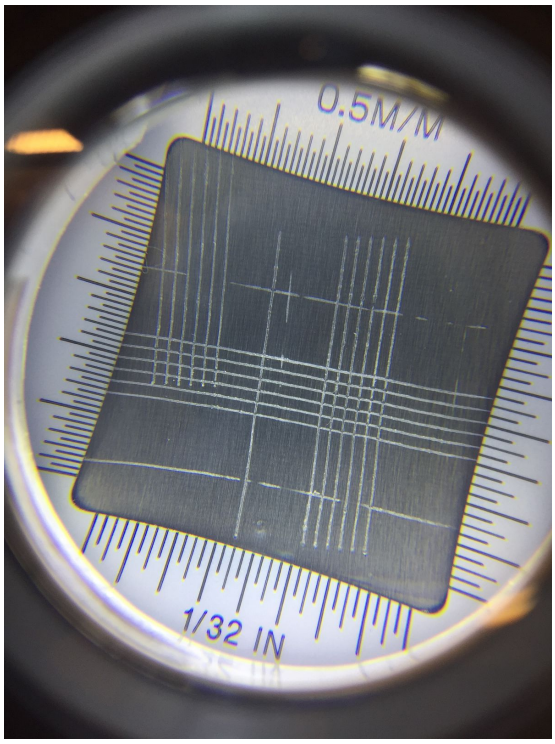

Figure 20: Magnified 5 x 5 grid on an E10 sample after tape was removed.

Pencil hardness testing (ASTM D3363[11]) was conducted with drafting pencils with hardnesses ranging from 6B (softest) to 6H (hardest). Before testing, each pencil was sharpened according to the guidelines presented in ASTM D3363[11]. For each pencil, the tip of the graphite was sanded to ensure the graphite was perfectly cylindrical. The pencil was then loaded into a BYK pencil hardness tester at a 45° angle and pushed across the surface of the coating at least 1 cm. All coatings were initially tested with the 6H pencil. Coatings were tested with increasingly softer pencils until a hardness was reached where the coating was not gouged by the pencil. The hardest pencil that did not gouge a given coating was reported as the coating's hardness. All testing was conducted by the same operator over the course of an hour to reduce the effects of temperature, humidity, and operator technique on the test results. **Figures 21 and 22** display top-down and side views (respectively) of the pencil hardness tester during a pencil hardness test.

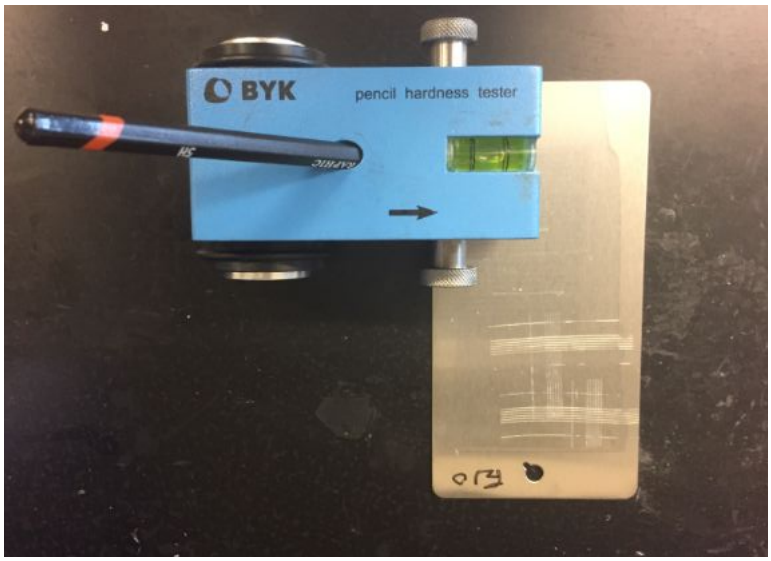

Figure 21: Top-down view of pencil hardness tester during test.

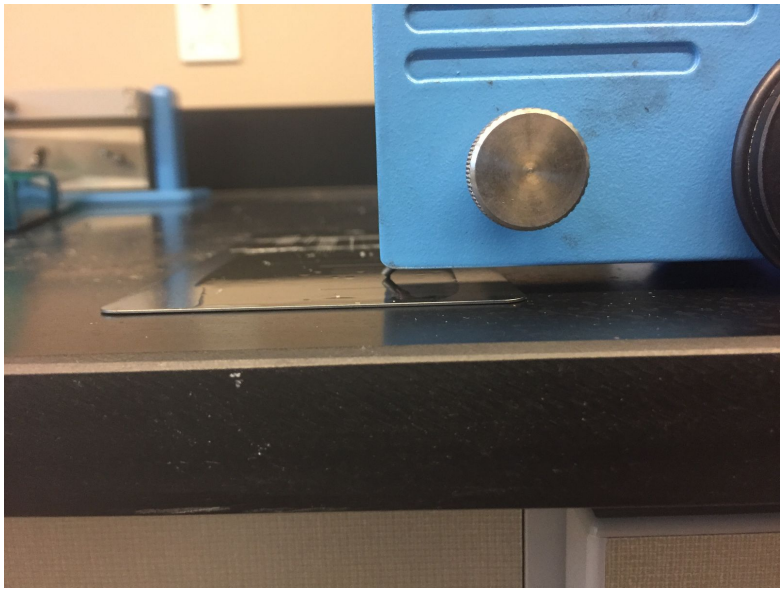

Figure 22: Side view of pencil hardness tester during test.

The König pendulum hardness test (Test Method A in ASTM D4366[10]) was conducted with a BYK pendulum hardness tester. For each coating, the sample was loaded so that the pendulum would pivot on the coating. The pendulum was released from a deflection of 6° and was timed until it damped to

a deflection of 3°. Due to possible variability in this test, each sample was evaluated in triplicate. Times were averaged to determine an average time for each coating. All testing was conducted by the same operator over the course of an hour to reduce the effects of temperature, humidity, and operator technique on the test results. **Figure 23** displays the pendulum tester. The location of the coated test panel is marked with a red arrow.

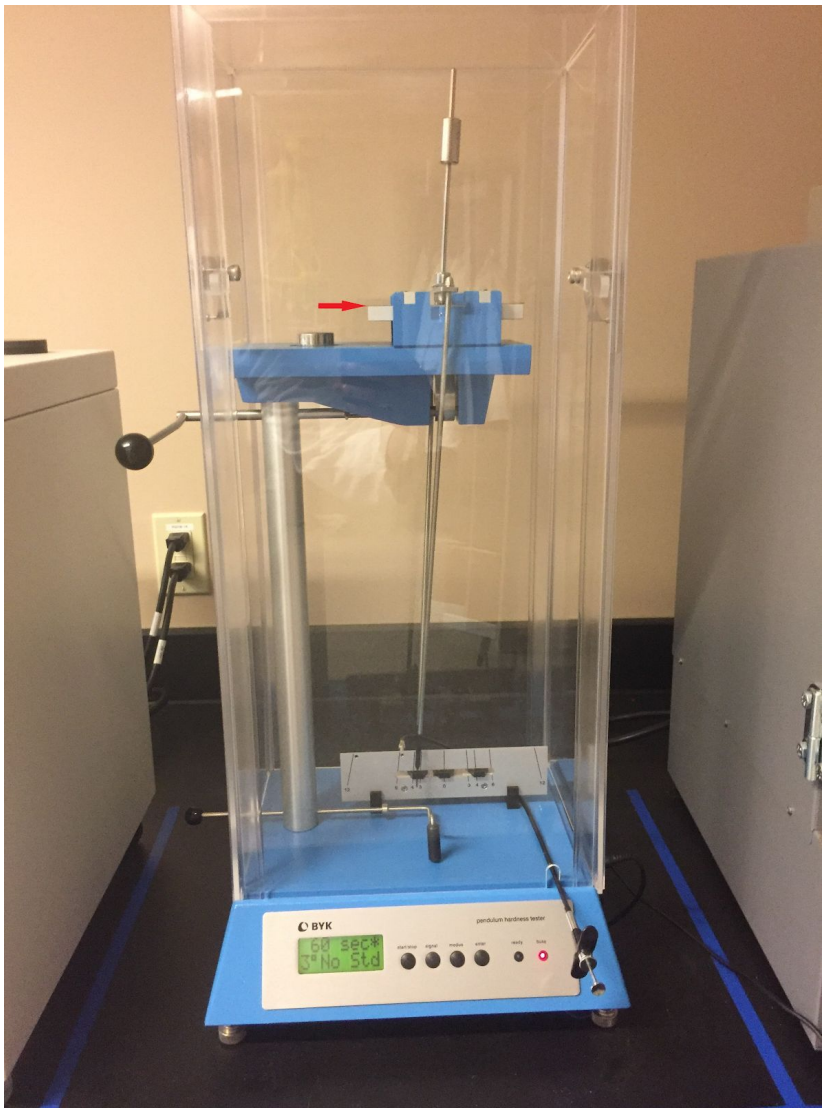

Figure 23: König pendulum hardness tester. Panel position is marked with red arrow.

The mandrel bend test (ASTM D522[12]) was used to evaluate coating flexibility. Coated panels were secured in the mandrel with three wingnuts and were positioned so that the end of the panel was at the small end of the mandrel. Coated panels were bent over the mandrel and then analyzed for cracking. Extent of cracking was correlated with **Figure 17** to determine each coating's percent elongation. **Figure 24** displays the conical mandrel used for flexibility testing.

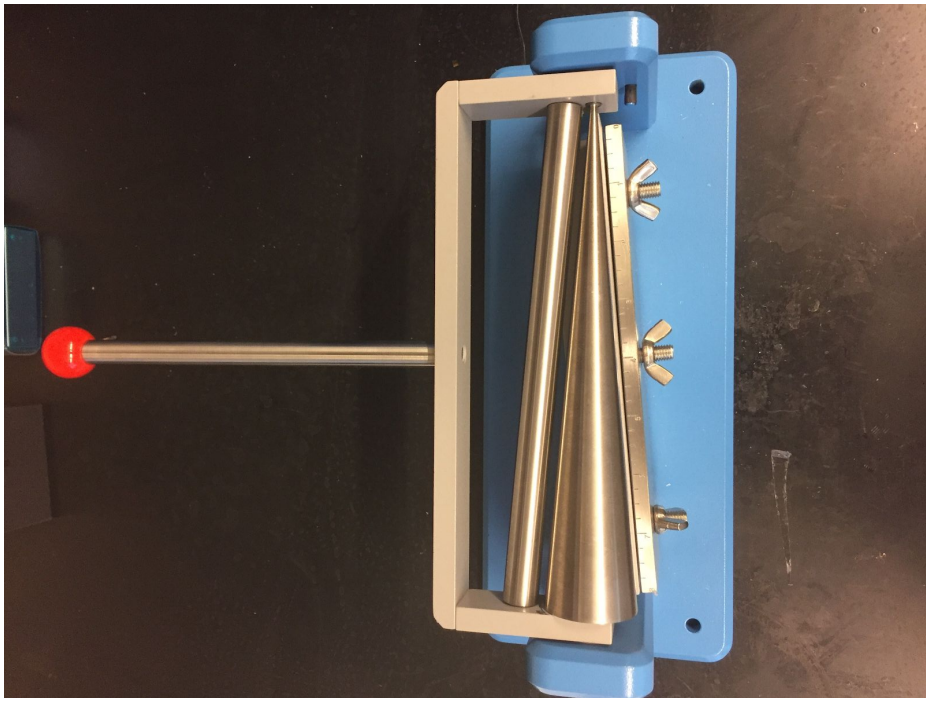

Figure 24: Conical mandrel used for flexibility testing. Panels were secured with wingnuts and bent over the mandrel.

Impact testing was conducted with a BYK-Gardner impact tester. The impact tester was used to drop a round 2 kg projectile on coated panels from a height of 100 cm. Testing was conducted with the projectile striking both the coated (forward impact test) and the uncoated (reverse impact test) sides of the panels. After testing, the coatings were inspected to determine if any cracking occurred as a result of the impact. In the event that cracking occurred, the projectile would be released from reduced heights until a

height was reached where the impact would not cause cracking. Impact test results were reported as a product of the projectile's mass and the projectile's initial height. **Figure 25** shows images of the impact tester. **Figure 26** shows an E30 coated panel after forward and reverse impact testing.

Figure 25: Images of the impact tester used for testing.

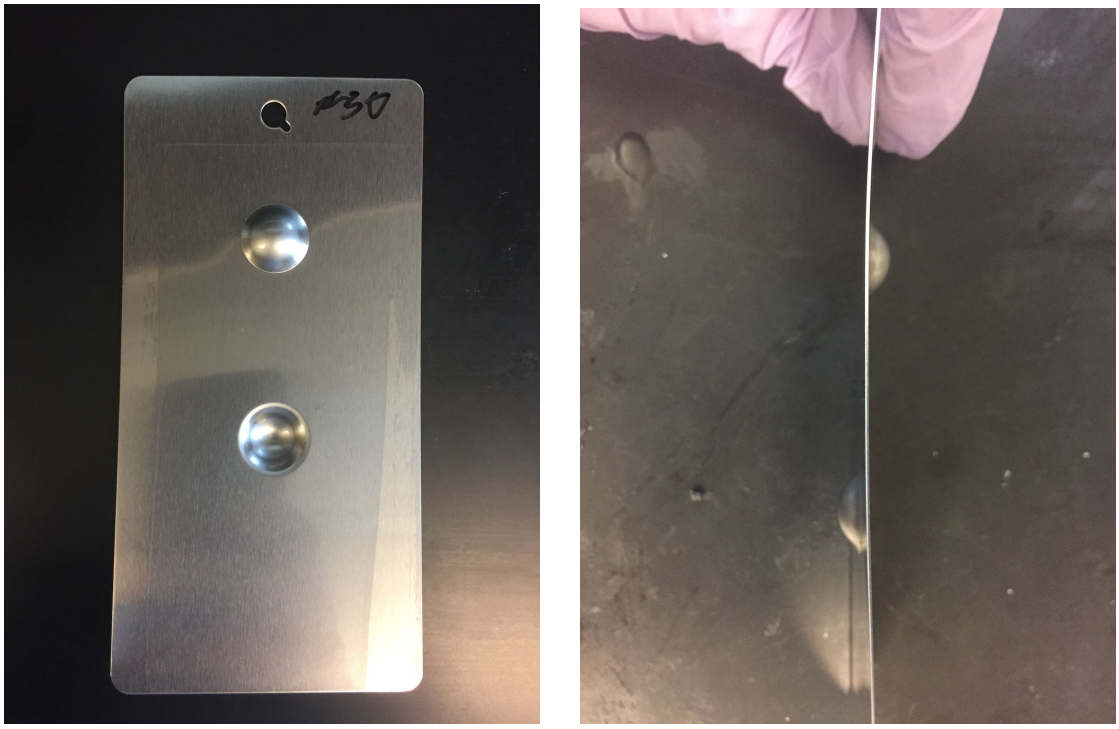

Figure 26: Images of an E30 coated panel subjected to forward and reverse impact testing.

5 Data and Results

5.1 EIS Data and Results

Testing was conducted according to the outlined experimental procedures. EIS testing was conducted multiple times on two coated panels for each epoxy coating. EIS data was plotted to form Nyquist and Bode plots on the Gamry Echem Analyst software. **Figures 27 and 28** illustrate Nyquist and Bode plots (respectively) for sample E0-1 (coating E0, panel 1) on the fourth day of EIS testing. These plots represent typical EIS plots for an intact coating. It is worth noting that the Bode plot has two sets of data plotted. On the Bode plot, the data points traced in red represent the plot of modulus (Z) versus frequency. The data points traced in blue represent the plot of alternating current phase angle versus frequency. Phase angle is not as important as modulus when determining the corrosion rate of a coated sample.

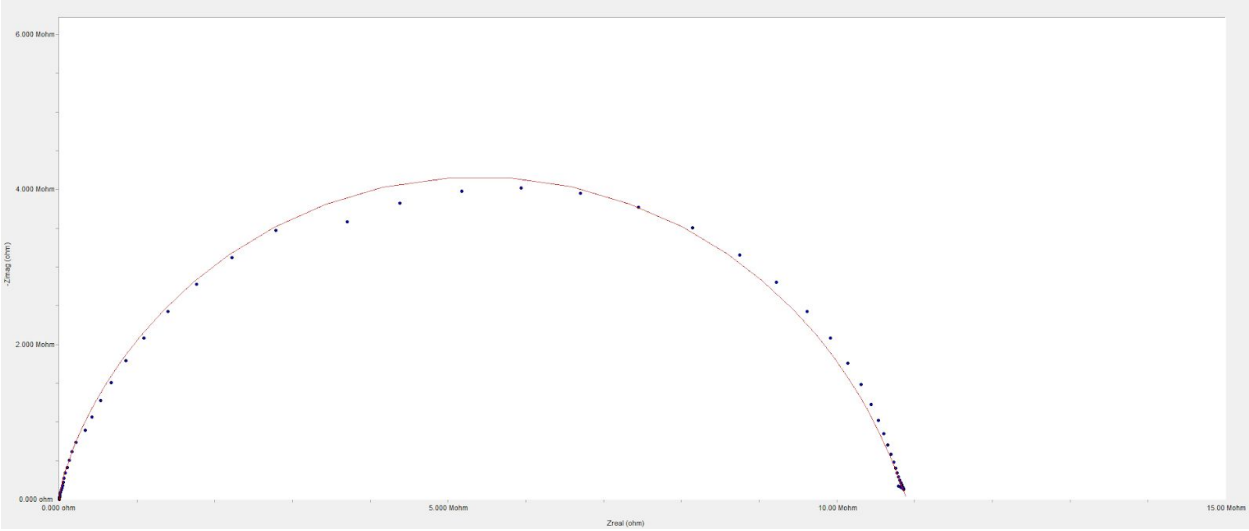

Figure 27: Nyquist plot for sample E0-1 on day 4 of testing.

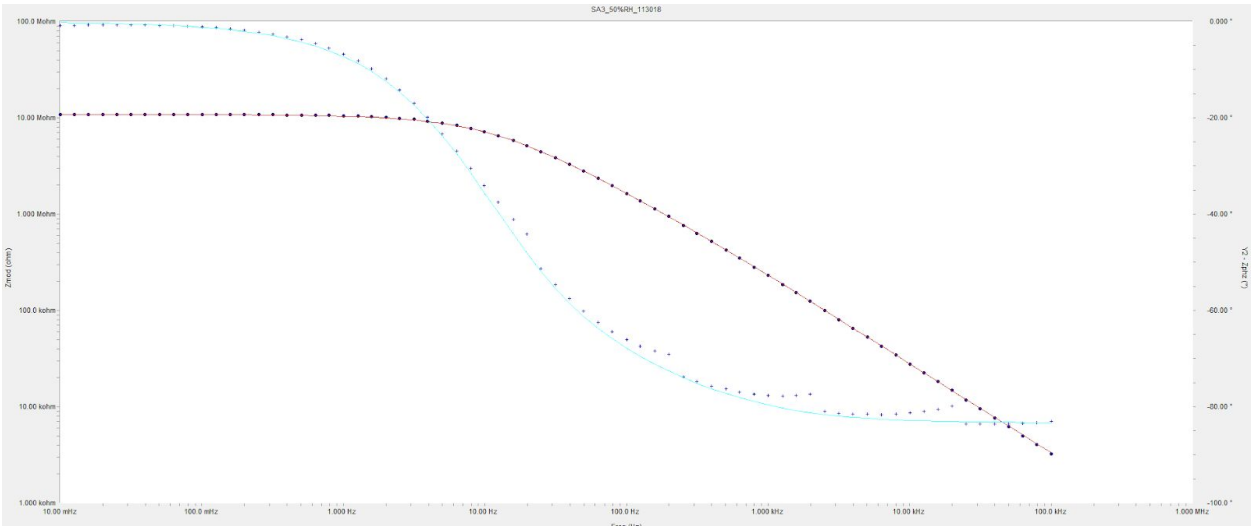

Figure 28: Bode plot for sample E0-1 on day 4 of testing. The data points traced in red represent the plot of modulus (Z) versus frequency. The data points traced in blue represent the plot of alternating current phase angle versus frequency.

For the most part, the Nyquist and Bode plots illustrated in **Figures 27 and 28** depict typical results encountered for the epoxy coated samples in this study. One notable exception was sample E20-2, whose Nyquist plot developed a second portion and whose Bode plot developed a different appearance in the low-frequency region as testing progressed. **Figures 29 and 30** display the Nyquist and Bode plots (respectively) for E20-2 at day 4. Early on in the testing, sample E20-2 behaved similarly to sample E0-1. As time progressed, sample E20-2 began to exhibit changes in its Nyquist and Bode plots. The changes in the Nyquist and Bode plots can be seen at day 67 in **Figures 31 and 32,** respectively.

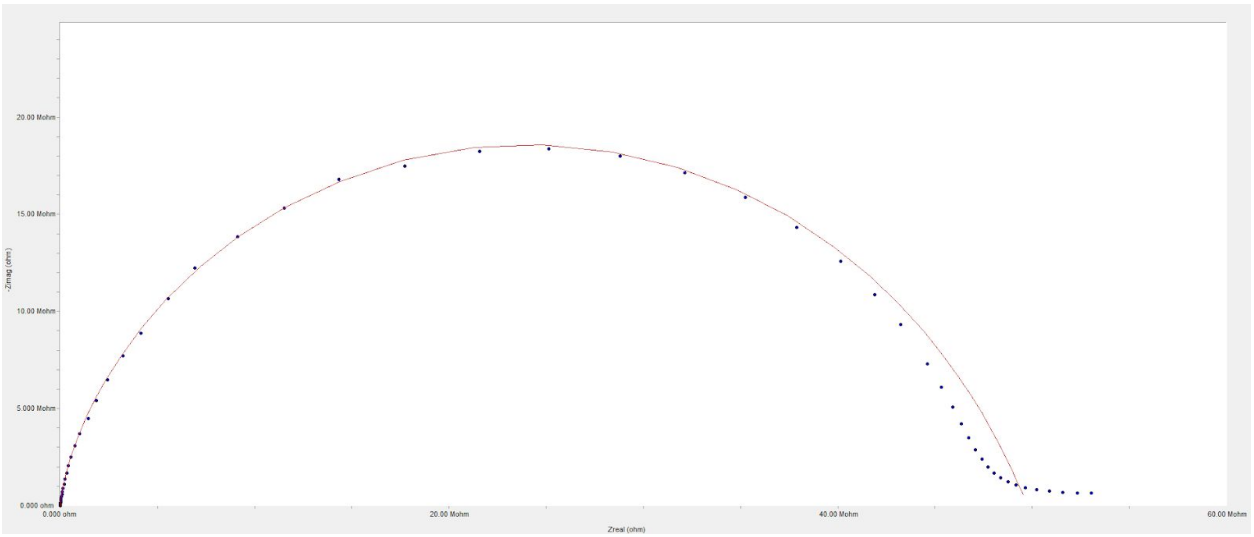

Figure 29: Nyquist plot for sample E20-2 at day 4.

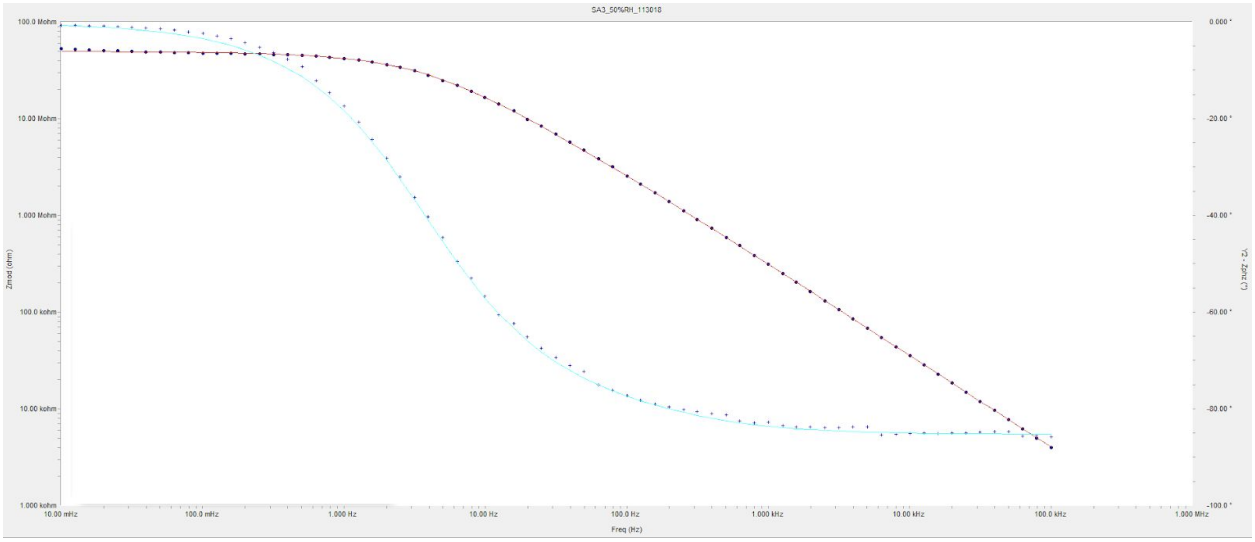

Figure 30: Bode plot for sample E20-2 at day 4.

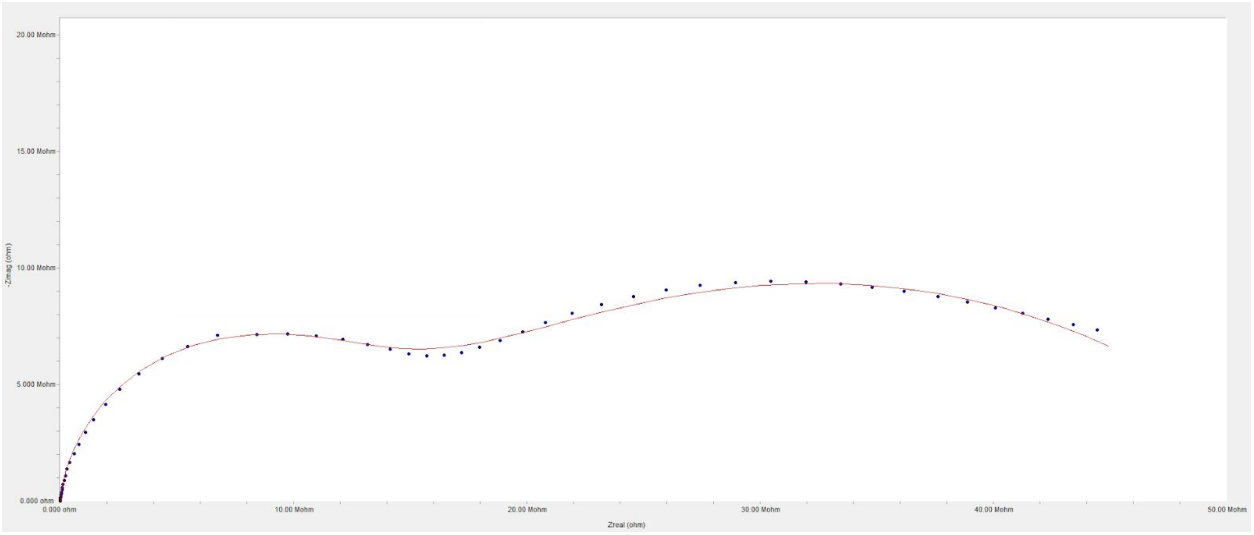

Figure 31: Nyquist plot for sample E20-2 at day 67.

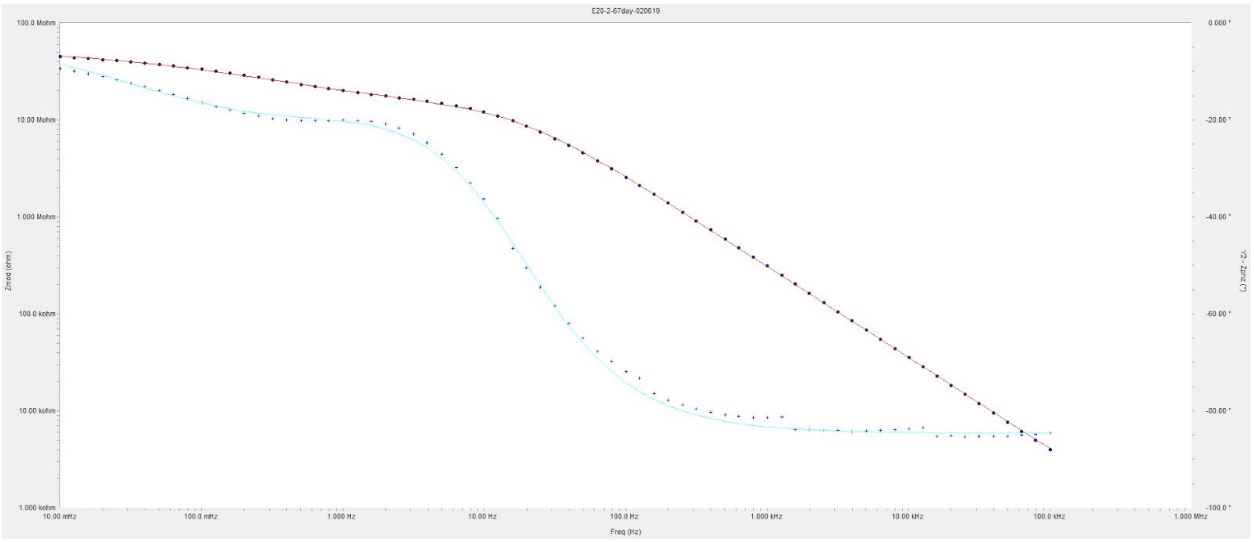

Figure 32: Bode plot for sample E20-2 at day 67. Note the more gradual decline of the modulus versus frequency plot (traced in red) in the low-frequency region of the plot.

Nyquist and Bode plots were analyzed to determine important parameters that could be related to corrosion rate. R_p and R_{coat} values were normalized by multiplying by the surface area of the coating exposed to the electrolyte (2.96 cm^2). R_s values were normalized by multiplying by the average distance

between the SCE reference electrode and the coated sample (2 cm). Since one sample developed significant defects (E20-2), it was fit to the equivalent circuit depicted in **Figure 10.** All other seven samples were fit to the equivalent circuit depicted in **Figure 9.** Data fit to the circuit depicted in **Figure 10** yield the following parameters: R_s, R_{coat}, Q_{coat} and the exponent associated with Q_{coat} (a_{coat}). R_{coat} can be treated like R_p for evaluating the corrosion protection provided by the coating. Data fit to the circuit depicted in **Figure 9** yield the following parameters: R_p, R_s, R_{pore}, Q_{coat}, Q_{dl}, and exponents associated with Q_{coat} and Q_{dl} (a_{coat} and a_{dl}, respectively). **Tables 2-9** summarize the EIS parameters for samples E0-1, E0-2, E10-1, E10-2, E20-1, E20-2, E30-1, and E30-2 (respectively) obtained over the course of many weeks.

Table 2: EIS parameters for E0-1. R_{coat} is analogous to R_p and can be used to evaluate corrosion protection.

Day	R_{coat} (Ω cm^2)	R_s (Ω cm)	Q_{coat} (S s^{acoat})	a_{coat}
1	2.36×10^{7}	3.83×10^{-3}	1.74×10^{-9}	8.99×10^{-1}
4	3.13×10^{7}	4.99×10^{-3}	1.88×10^{-9}	8.92×10^{-1}
46	3.30×10^{7}	6.51×10^{-3}	2.21×10^{-9}	8.82×10^{-1}
53	3.19×10^{7}	1.54×10^{-2}	2.23×10^{-9}	8.82×10^{-1}
67	2.93×10^{7}	1.70×10^{-2}	2.29×10^{-9}	8.80×10^{-1}
74	2.92×10^{7}	2.75×10^{-2}	2.29×10^{-9}	8.81×10^{-1}
81	3.11×10^{7}	3.61×10^{-2}	2.26×10^{-9}	8.81×10^{-1}
88	2.97×10^{7}	8.38×10^{-2}	2.30×10^{-9}	8.80×10^{-1}

Table 3: EIS parameters for E0-2.

Day	R_{coat} (Ω cm^2)	R_s (Ω cm)	Q_{coat} (S s^{acoat})	a_{coat}
1	2.25×10^{7}	1.60×10^{-2}	1.64×10^{-9}	9.01×10^{-1}
4	1.80×10^{7}	3.56×10^{-2}	1.67×10^{-9}	9.00×10^{-1}
46	2.89×10^{7}	8.50×10^{-2}	2.10×10^{-9}	8.84×10^{-1}
53	2.92×10^{7}	6.91×10^{-2}	2.11×10^{-9}	8.84×10^{-1}
67	2.66×10^{7}	1.25×10^{-1}	2.20×10^{-9}	8.81×10^{-1}
74	2.66×10^{7}	1.16×10^{-1}	2.22×10^{-9}	8.80×10^{-1}
81	2.77×10^{7}	1.25×10^{-1}	2.23×10^{-9}	8.80×10^{-1}
88	2.67×10^{7}	6.75×10^{-2}	2.24×10^{-9}	8.79×10^{-1}

Table 4: EIS parameters for E10-1.

Day	R_{coat} (Ω cm^2)	R_s (Ω cm)	Q_{coat} (S s^{acoat})	a_{coat}
1	3.82×10^{7}	3.80×10^{-4}	1.48×10^{-9}	9.04×10^{-1}
4	6.95×10^{7}	6.13×10^{-4}	1.40×10^{-9}	9.05×10^{-1}
46	7.92×10^{7}	9.92×10^{-4}	1.54×10^{-9}	9.00×10^{-1}
53	7.70×10^{7}	7.14×10^{-5}	1.53×10^{-9}	9.01×10^{-1}
67	7.83×10^{7}	1.42×10^{-4}	1.53×10^{-9}	9.01×10^{-1}
74	7.64×10^{7}	3.04×10^{-4}	1.54×10^{-9}	9.00×10^{-1}
81	9.35×10^{7}	7.73×10^{-4}	1.51×10^{-9}	9.01×10^{-1}
88	9.08×10^{7}	1.52×10^{-2}	1.51×10^{-9}	9.02×10^{-1}

Table 5: EIS parameters for E10-2.

Day	R_{coat} (Ω cm^2)	R_s (Ω cm)	Q_{coat} (S s^{acoat})	a_{coat}
1	4.00×10^{7}	3.82×10^{-6}	2.94×10^{-9}	9.03×10^{-1}
4	6.35×10^{7}	6.81×10^{-3}	2.80×10^{-9}	9.08×10^{-1}
46	7.26×10^{7}	7.02×10^{-3}	2.80×10^{-9}	9.06×10^{-1}
53	6.87×10^{7}	1.07×10^{-2}	2.81×10^{-9}	9.06×10^{-1}
67	9.07×10^{7}	2.79×10^{-2}	2.86×10^{-9}	9.05×10^{-1}
74	8.70×10^{7}	6.44×10^{-2}	2.89×10^{-9}	9.04×10^{-1}
81	9.52×10^{7}	6.38×10^{-2}	2.85×10^{-9}	9.04×10^{-1}
88	8.79×10^{7}	3.99×10^{-2}	2.96×10^{-9}	9.02×10^{-1}

Table 6: EIS parameters for E20-1.

Day	R_{coat} (Ω cm^2)	R_s (Ω cm)	Q_{coat} (S s^{acoat})	a_{coat}
1	8.06×10^{7}	1.33×10^{-1}	1.15×10^{-9}	9.14×10^{-1}
4	1.52×10^{8}	1.73×10^{-1}	1.10×10^{-9}	9.16×10^{-1}
46	2.97×10^{8}	1.83×10^{-1}	1.08×10^{-9}	9.17×10^{-1}
53	2.89×10^{8}	2.61×10^{-1}	1.06×10^{-9}	9.17×10^{-1}
67	2.60×10^{8}	3.20×10^{-1}	1.08×10^{-9}	9.16×10^{-1}
74	2.57×10^{8}	4.29×10^{-1}	1.09×10^{-9}	9.16×10^{-1}
81	2.67×10^{8}	2.92×10^{-1}	1.08×10^{-9}	9.16×10^{-1}
88	2.59×10^{8}	1.15×10^{-3}	1.09×10^{-9}	9.16×10^{-1}

Table 7: EIS parameters for E20-2. Days marked with an asterisk (*) are days for which data was fit to the circuit in **Figure 9**. Therefore, the entries in the R_p column are for R_{coat} values.

Day	R_p (Ω cm^2)	R_{pore} (Ω cm^2)	R_s (Ω cm)	Q_{coat} (S s^{acoat})	a_{coat}	Q_{dl} (S s^{adl})	a_{dl}
1*	7.84×10^{7}	-	1.22×10^{-2}	1.17×10^{-9}	9.14×10^{-1}	-	-
4*	1.39×10^{8}	-	2.20×10^{-2}	1.13×10^{-9}	9.16×10^{-1}	-	-
46	1.41×10^{8}	4.61×10^{7}	2.09×10^{-3}	8.57×10^{-10}	9.41×10^{-1}	3.54×10^{-8}	5.35×10^{-1}
53	1.35×10^{8}	4.32×10^{7}	2.64×10^{-3}	8.54×10^{-10}	9.41×10^{-1}	3.40×10^{-8}	5.30×10^{-1}
67	1.21×10^{8}	3.98×10^{7}	3.52×10^{-3}	8.69×10^{-10}	9.40×10^{-1}	3.64×10^{-8}	5.25×10^{-1}
74	1.22×10^{8}	3.87×10^{7}	2.64×10^{-3}	8.62×10^{-10}	9.40×10^{-1}	3.73×10^{-8}	5.15×10^{-1}
81	1.28×10^{8}	3.70×10^{7}	6.28×10^{-3}	8.60×10^{-1}	9.41×10^{-1}	4.09×10^{-8}	4.86×10^{-1}
88	1.25×10^{8}	3.89×10^{7}	1.37×10^{-1}	8.89×10^{-10}	9.38×10^{-1}	5.93×10^{-8}	5.04×10^{-1}

Table 8: EIS parameters for E30-1.

Day	R_{coat} (Ω cm^2)	R_s (Ω cm)	Q_{coat} (S s^{acoat})	a_{coat}
1	1.59×10^{8}	3.56×10^{-2}	9.39×10^{-10}	9.20×10^{-1}
4	3.86×10^{8}	3.26×10^{-2}	8.57×10^{-10}	9.24×10^{-1}
46	9.04×10^{8}	2.68×10^{-3}	7.94×10^{-10}	9.28×10^{-1}
53	9.19×10^{8}	5.32×10^{-3}	7.94×10^{-10}	9.29×10^{-1}
67	9.54×10^{8}	1.22×10^{-2}	8.06×10^{-10}	9.27×10^{-1}
74	9.39×10^{8}	1.60×10^{-2}	8.12×10^{-10}	9.26×10^{-1}
81	9.69×10^{8}	2.07×10^{-2}	8.13×10^{-10}	9.26×10^{-1}
88	9.59×10^{8}	5.15×10^{-4}	8.13×10^{-10}	9.26×10^{-1}

Table 9: EIS parameters for E30-2.

Day	R_{coat} (Ω cm^2)	R_s (Ω cm)	Q_{coat} (S s^{acoat})	a_{coat}
1	1.52×10^{8}	1.07×10^{-1}	9.67×10^{-10}	9.20×10^{-1}
4	3.89×10^{8}	2.29×10^{-2}	8.41×10^{-10}	9.29×10^{-1}
46	7.59×10^{8}	9.73×10^{-3}	7.58×10^{-10}	9.35×10^{-1}
53	7.62×10^{8}	1.01×10^{-2}	7.80×10^{-10}	9.32×10^{-1}
67	7.94×10^{8}	1.65×10^{-2}	7.85×10^{-10}	9.32×10^{-1}
74	7.59×10^{8}	4.03×10^{-2}	7.88×10^{-10}	9.32×10^{-1}
81	7.46×10^{8}	5.48×10^{-2}	7.67×10^{-10}	9.34×10^{-1}
88	7.20×10^{8}	3.81×10^{-4}	7.69×10^{-10}	9.34×10^{-1}

5.2 Mechanical Testing Data and Results

Tape adhesion testing was conducted twice for each coating to reduce the effects of experimental error on the results. **Table 10** displays results of the tape adhesion test. All coatings were classified as 5B except for Trial 1 for coating E10.

Table 10: Tape adhesion test results for the epoxy coatings.

Coating	Trial 1	Trial 2
E0	5B	5B
E10	4B	5B
E20	5B	5B
E30	5B	5B

Table 11 contains results for the pencil hardness test. Sample E30 had a gouge hardness of 4H, samples E20 and E10 had gouge hardnesses of 5H, and E0 had a gouge hardness greater than the hardest pencil tested (6H).

Table 11: Pencil hardness test results for the epoxy coatings.

Coating	Gouge Hardness
E0	> 6H
E10	5H
E20	5H
E30	4H

The pendulum hardness test was conducted three times for each coating to reduce variation. The three values for each coating were averaged. **Table 12** contains the results for the pendulum hardness tests and the average times for each coating.

Table 12: Pendulum hardness test times and average times for each epoxy coating.

Coating	Trial 1 (s)	Trial 2 (s)	Trial 3 (s)	Average (s)
E0	168	166	164	166.0
E10	152	150	147	149.7
E20	140	139	138	139.0
E30	103	103	103	103.0

The results of the mandrel bend flexibility test were correlated to the percent elongation of each coating. **Table 13** lists the results of the mandrel bend tests. No coatings cracked during the test, so the percent elongation of each sample was listed as > 32% (32% is the maximum value that can be correlated from the test).

Table 13: Percent elongation results for each epoxy coating obtained from the mandrel bend test.

Coating	Percent Elongation
E0	>32%
E10	>32%
E20	>32%
E30	>32%

As previously mentioned, both forward and reverse impact testing was conducted. **Table 14** lists the forward and reverse impact test results. No cracking was observed on any of the coatings for either of the test orientations, so the impact values were listed as > 200 kg cm (200 kg cm is the maximum reading achievable on the BYK-Gardner impact tester).

Table 14: Forward and reverse impact test results for the epoxy coatings.

Coating	Forward Impact	Reverse Impact
E0	>200 kg cm	>200 kg cm
E10	>200 kg cm	>200 kg cm
E20	>200 kg cm	>200 kg cm
E30	>200 kg cm	>200 kg cm

6 Discussion, Analysis, and Conclusions

6.1 Analysis and Discussion of EIS Results

The epoxy coatings' level of corrosion protection can be determined by analyzing polarization resistance (R_p) values. As mentioned previously, R_p and corrosion rate are inversely proportional. In other words, corrosion rate decreases as R_p increases. From the onset of the EIS testing on day 1, the epoxy coatings had increasing R_p values (and decreasing corrosion rate) as the CGE content increased. This result can most easily be seen in **Figures 33 and 34,** which compare the Nyquist and Bode plots (respectively) for all eight samples on day 1. As evidenced in **Figure 33,** the two E30 samples had the largest semicircle plots (and therefore the largest initial R_p values) and the two E0 samples had the smallest semicircle plots. In **Figure 34,** the two E30 samples had the highest moduli (and therefore the largest initial R_p values) and the two E0 samples had the smallest moduli. These observations suggest that E30 offered the greatest corrosion protection initially and that corrosion protection increased as CGE content increased.

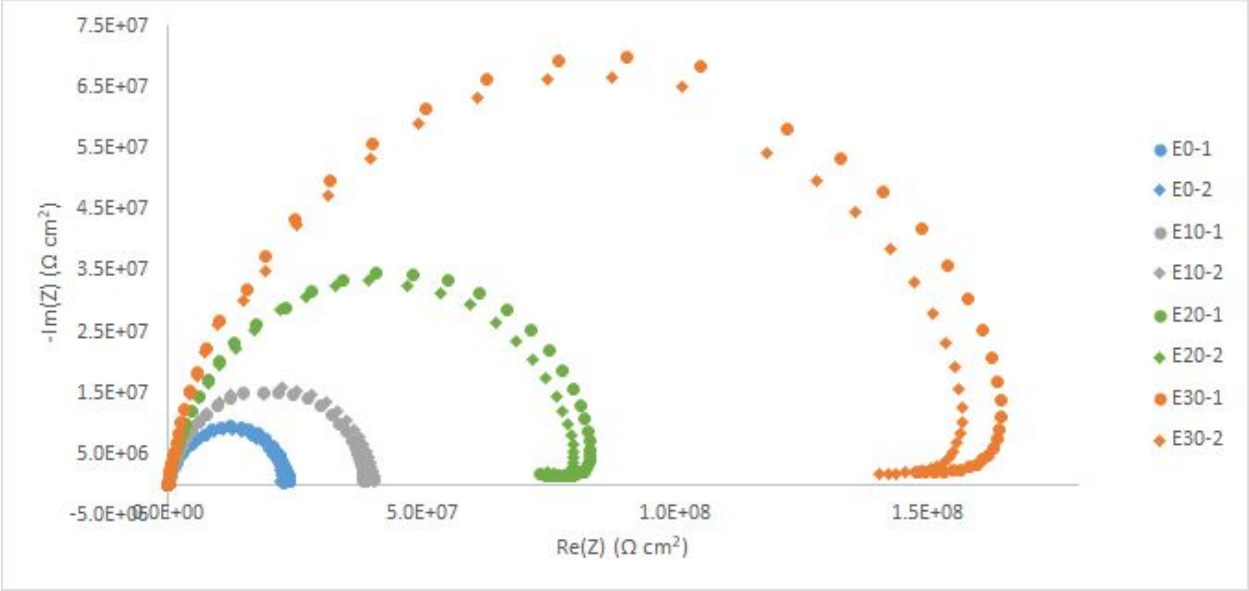

Figure 33: Comparison of Nyquist plots for the eight samples on day 1. Note that the E30 samples had the greatest R_p values and that the E0 samples had the smallest R_p values.

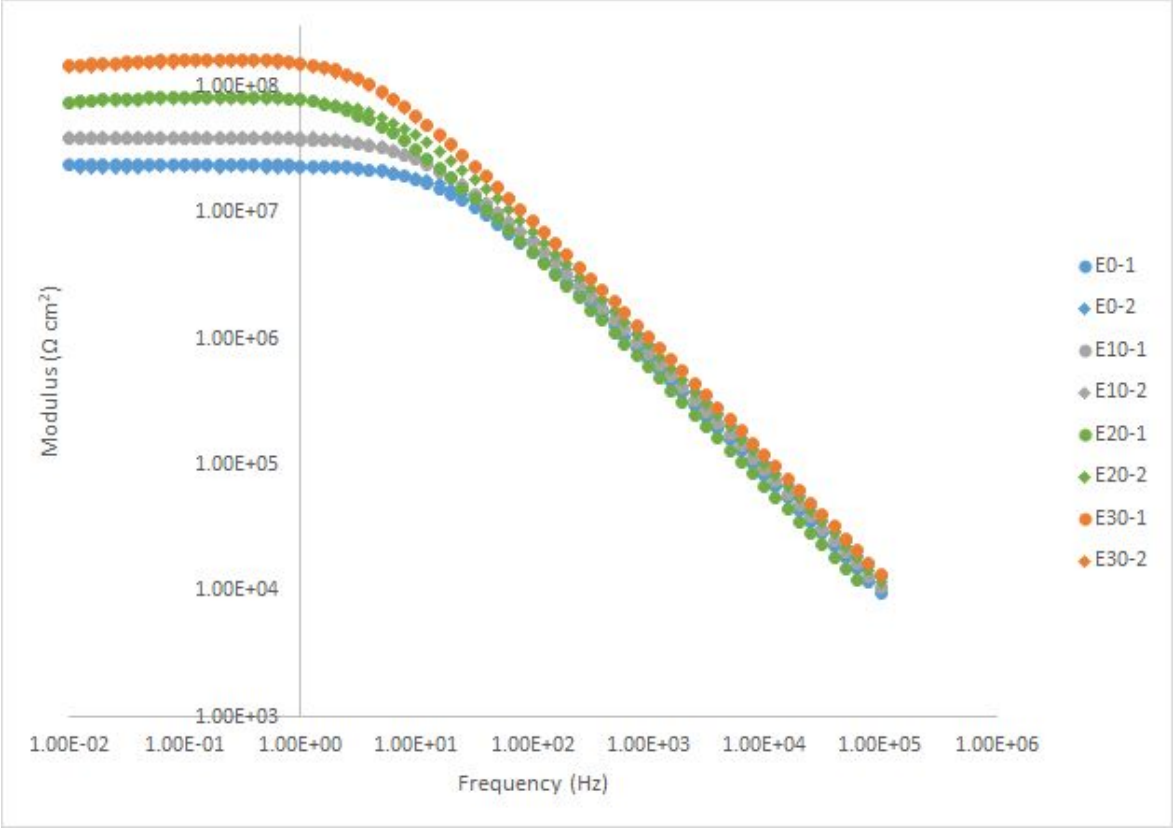

Figure 34: Comparison of Bode plots for the eight samples on day 1. Note that the E30 samples had the greatest R_p values and that the E0 samples had the smallest R_p values.

On day 4, the coatings all exhibited greater R_p values than they did on day 1. This could be due to some phenomenon occurring on the surfaces of the coatings. As time progressed, reactants for the corrosion cathodic reactions may have become depleted near the surface of the coating. Species (such as dissolved oxygen gas) becoming depleted near the coating surface would cause a lower corrosion rate. This is consistent with the observation of greater R_p values, since greater R_p values corresponds to lower corrosion rates. This suggests that the dominant corrosion reactions may be dependent on reactions like the oxygen reduction reaction. However, further investigation is required to determine whether or not this is the case.

As was the case for day 1, the E30 samples exhibited the greatest R_p values and the E0 samples exhibited the smallest R_p values. **Figures 35 and 36** display the Nyquist and Bode plots (respectively) for the eight coated samples on day 4.

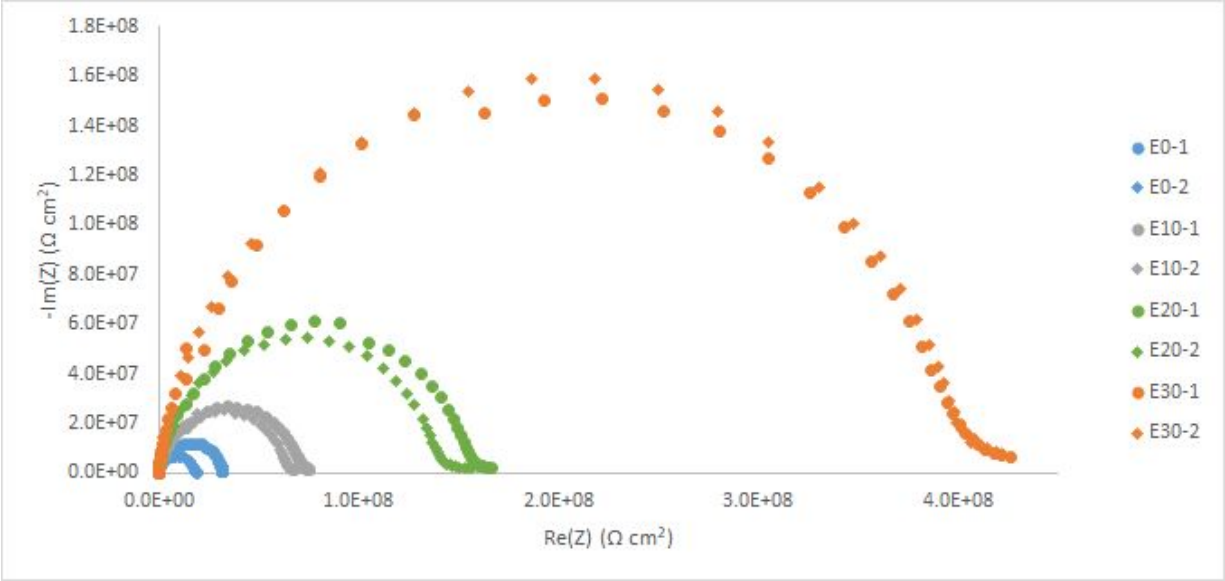

Figure 35: Comparison of Nyquist plots for the eight samples on day 4.

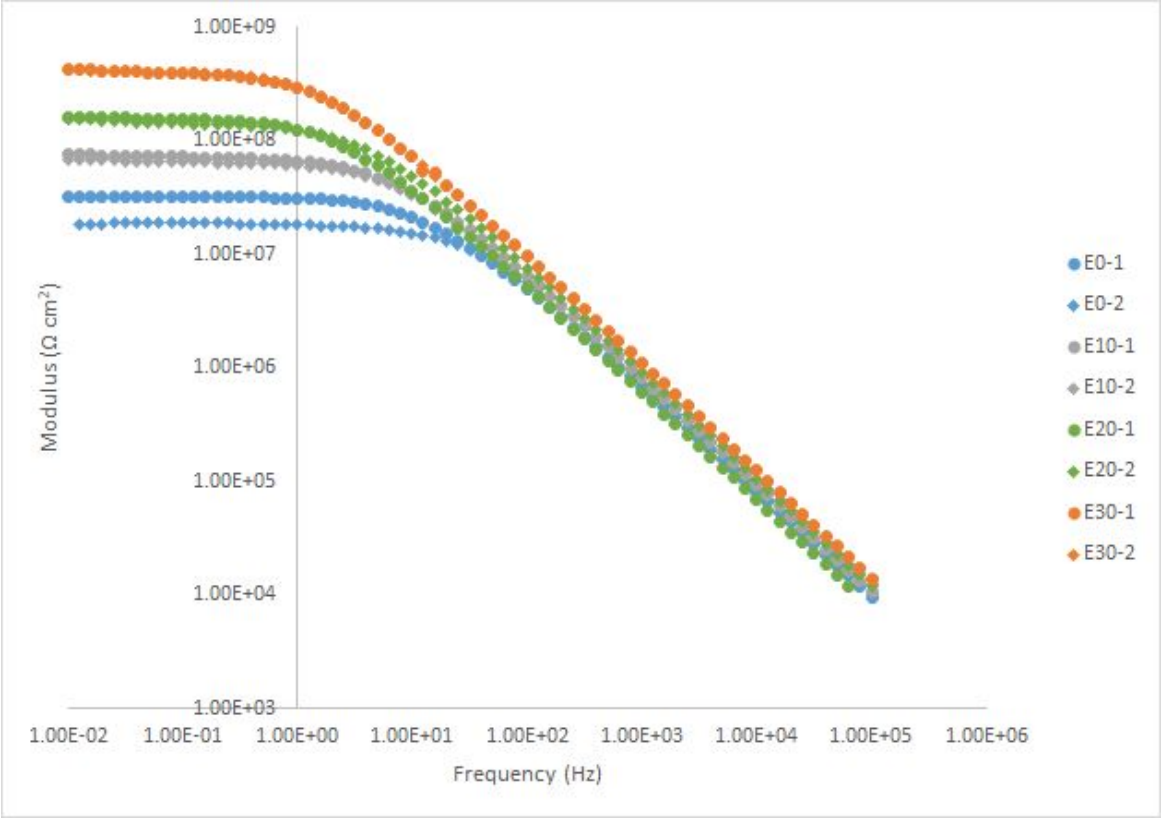

Figure 36: Comparison of Bode plots for the eight samples on day 4.

By day 53, samples had sufficient time to begin to diverge from each other. At day 53, the two E30 samples had somewhat different R_p values. This could be due to small defects in the coatings or variations in the coatings' thickness. The impact of the differences between the E30 samples evidently took several weeks to manifest. The most significant difference is the change in sample E20-2. The Nyquist plot for E20-2 displays the formation of an additional semicircle "hump." The Bode plot for E20-2 displays a more gradual decrease in modulus at low frequency when compared to the Bode plot for E20-1. The changes in the Nyquist and Bode plots suggests the formation of a significant defect in E20-2. The presence of a defect means that the coating provides less corrosion protection than an intact coating since the electrolyte is able to reach the metal substrate. More likely than not, the electrolyte finally broke through an air bubble that was present in the coating when it was applied to the metal test panel. A

cursory inspection of E20-2 did not yield any visual evidence of a defect, though it may be small or in a location where it is not easily seen. Once EIS testing is complete, a more thorough examination of E20-2 can be conducted.

On day 53, the E30 samples exhibited the greatest R_p values and the E0 samples exhibited the smallest R_p values. As was observed at day 4, the R_p values had generally increased as time progressed. It is worth noting that even though E20-2 developed a defect, its R_p value was similar to those of the E10 samples. **Figures 37 and 38** display the Nyquist and Bode plots (respectively) for the eight coated samples on day 53.

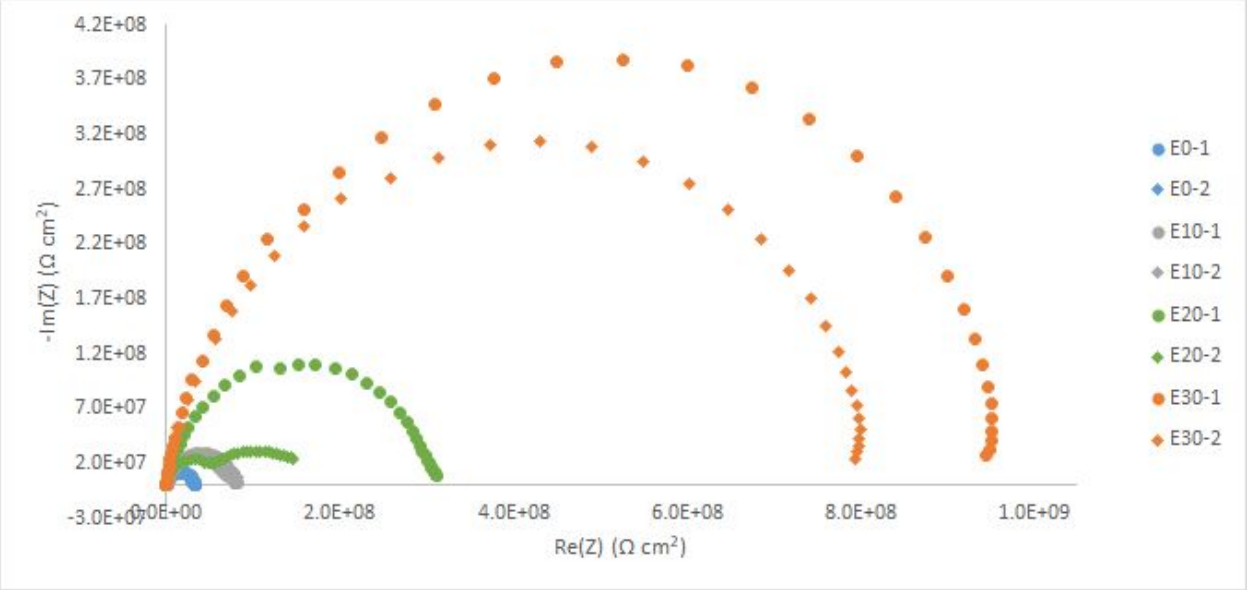

Figure 37: Comparison of Nyquist plots for the eight samples on day 53.

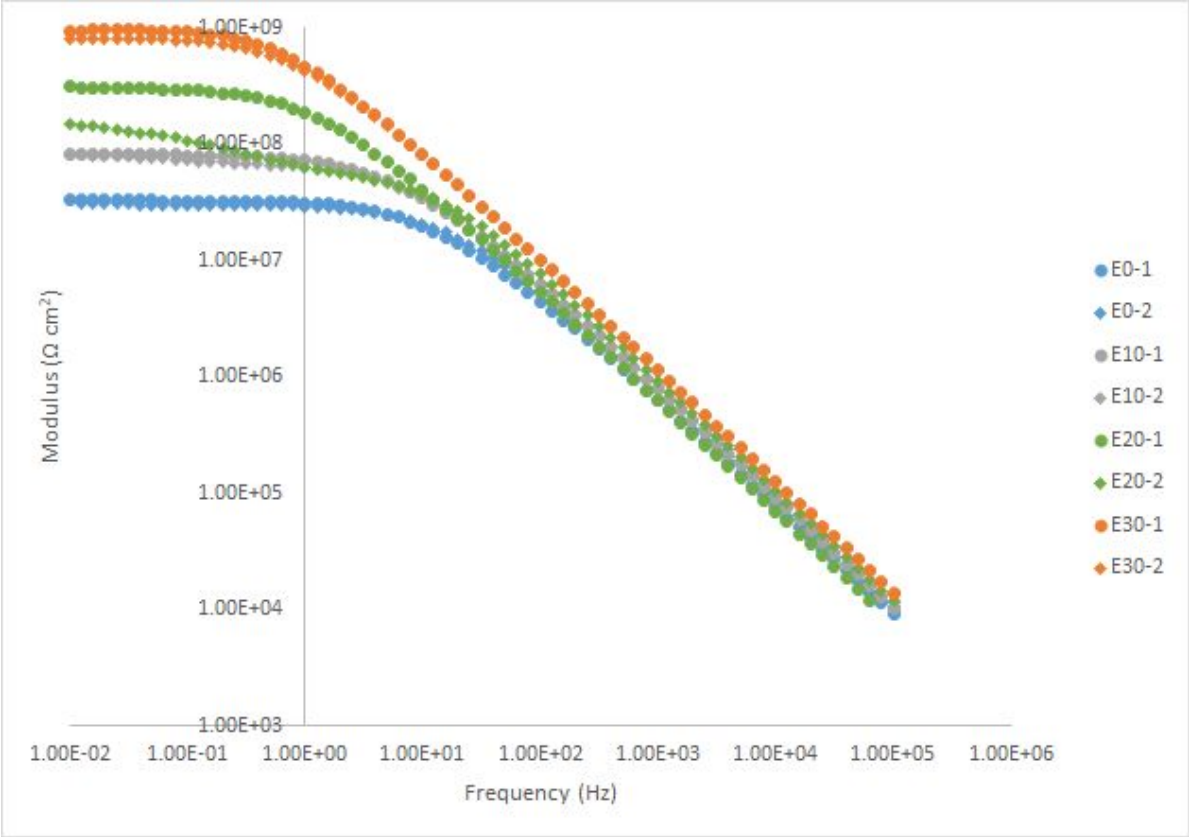

Figure 38: Comparison of Bode plots for the eight samples on day 53.

On day 81, the samples still exhibited a general increasing trend in their R_p values. The two E30 samples had significantly larger R_p values than the E0, E10, and E20 samples had. Sample E20-2 still displayed the same behavior that suggested the presence of a defect in the coating. In fact, it had a lower R_p value than both E10 samples, indicating that it offered worse corrosion protection than the E10 samples. **Figures 39 and 40** display the Nyquist and Bode plots (respectively) for the eight samples on day 81.

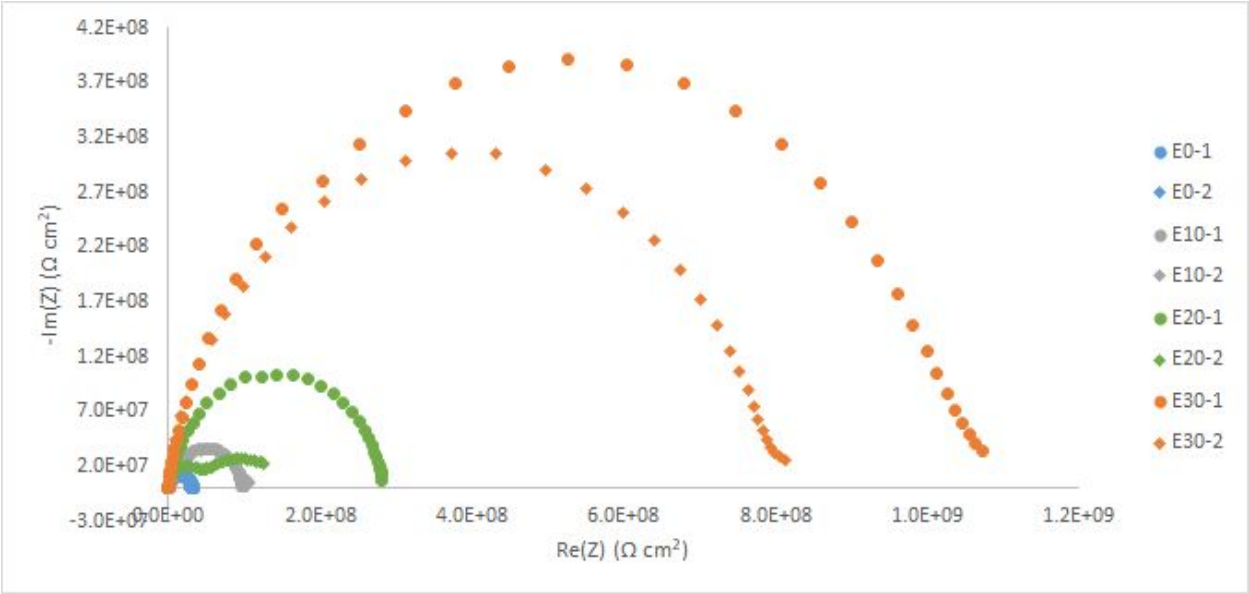

Figure 39: Comparison of Nyquist plots for the eight samples on day 81.

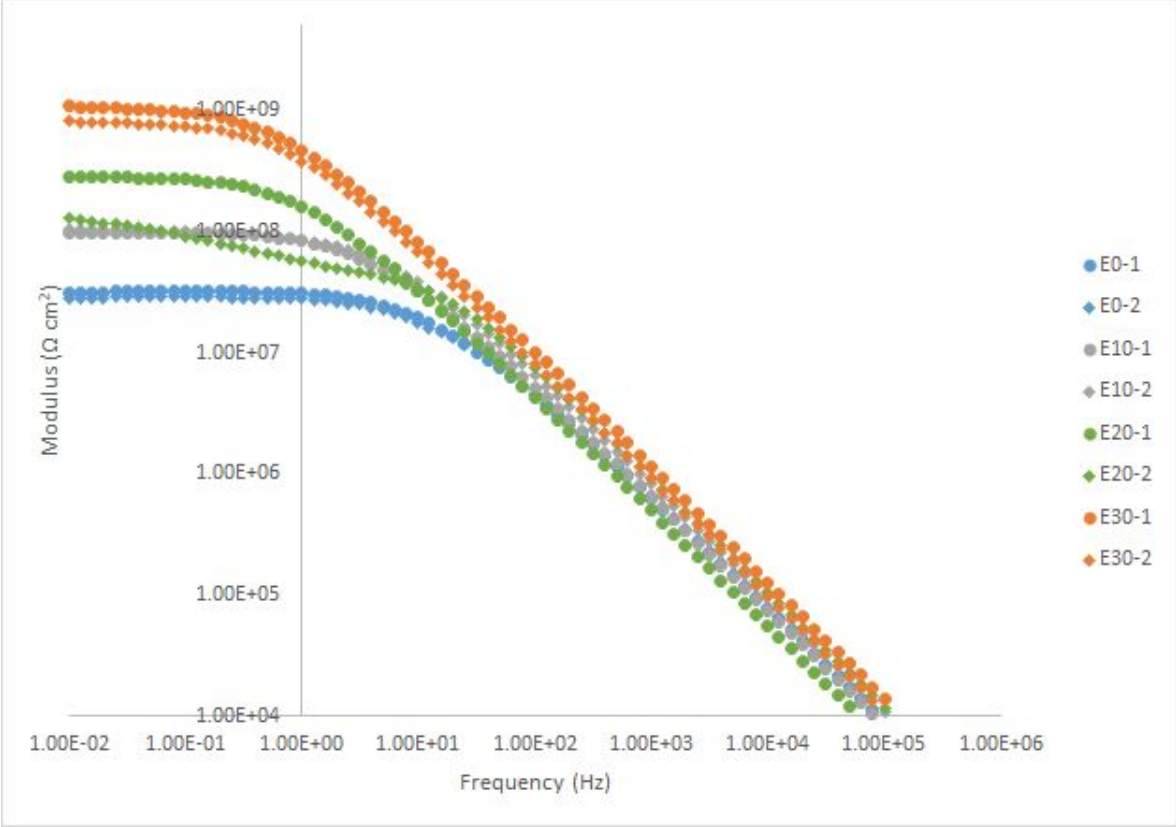

Figure 40: Comparison of Bode plots for the eight samples on day 81.

EIS testing provided information that can be used to determine the corrosion protection provided by each coating. E0 (the coating formulated with only TMPGE) consistently had the lowest R_p values over the course of the EIS tests. E10 (the coating formulated with CGE replacing some of the TMPGE) had the next lowest R_p values. E20 (the coating formulated with CGE replacing most of the TMPGE) had the second highest R_p values before E20-2 developed a defect. E20-1 continued to perform well, which suggests that if E20-2 had not developed a defect, it would have continued to perform well. Since the defect is possibly cause by an air bubble formed when the coating was applied, a more optimized application procedure may reduce the chances of defects forming.

E30 (the coating formulated with only CGE) consistently had the greatest R_p values over the duration of EIS testing. On day 1, the R_p values for the E30 samples were roughly 5 times that of the E0 samples. On day 4, the R_p values for the E30 samples were roughly 12 times that of the E0 samples. On day 53, the R_p values for the E30 samples were roughly 25 times that of the E0 samples. On day 81, the R_p values for the E30 samples were roughly 30 times that of the E0 samples. The R_p values for the E0 samples were more consistent over time than the R_p values of the E30 samples were (which tended to increase over time), but the E30 samples still had significantly greater R_p values than the E0 samples even when the E30 samples' R_p values were at their lowest. These results suggest that substituting CGE for TMPGE greatly enhanced the corrosion protection provided by the epoxy coating.

6.2 Analysis and Discussion of Mechanical Testing Results

The results of the mechanical testing were less drastically different between the coatings. All coatings exhibited excellent adhesion during the tape adhesion test. Only one coating, E10, exhibited any coating loss. This loss was very minor (the coating earned the 4B classification), and upon repeating the test, the E10 sample lost no coating (earning the 5B classification). The other three coatings (E0, E20, and E30) earned the 5B classification both times they were tested.

Some differences in coating hardness were observed. In the pencil hardness test, E0 was the hardest coating (with a hardness greater than 6H), E10 and E20 were the next hardest coatings (5H), and E30 was the least hard coating (4H). This suggests that substituting CGE for TMPGE decreased the hardness of the coating.

Similar results were observed for the pendulum hardness test. E0 had the longest average test end time (166.0 s), which indicates that it was the hardest coating tested. E10 had the second longest average test end time (149.7 s). E20 had the third longest average test end time (139.0 s). E30 had the shortest average test end time (103.0 s), which indicates that it was the softest coating tested. As was indicated by the pencil hardness test, substituting CGE for TMPGE likely decreased coating hardness.

No significant differences were observed between the coatings in the conical mandrel bend test. No cracking was observed on any of the coatings, and each coating earned an elongation percentage of >32%. This indicates that all of the coatings tested had excellent flexibility. The results suggest that substituting CGE for TMPGE had no measurable effect on the flexibility of the coating.

No significant differences were observed between the coatings in the forward and reverse impact tests. No cracking was observed on any of the coatings for forward and reverse impacts, and each coating earned an impact value of >200 kg cm. This indicates that all of the coatings tested had excellent impact resistance. The results suggest that substituting CGE for TMPGE had no measurable effect on the impact resistance of the coating.

As discussed previously, no single coating outperformed all of the other coatings in every test. Substituting CGE for TMPGE as the reactive diluent had the positive effect of greatly improving corrosion protection, but had a negative impact on coating hardness. Using only TMPGE as the reactive diluent conferred good coating hardness, but reduced the degree of corrosion protection. Coatings formulated with both CGE and TMPGE had moderate hardnesses and degrees of corrosion protection. No measurable differences in flexibility, adhesion, and impact resistance were observed within the scope of

the tests conducted. In general, the study suggested that corrosion protection increased and hardness decreased as the amount of CGE increased.

It is not possible to decide which of the four coatings is the best without considering which application they may be used for. If the application primarily requires excellent corrosion protection, then a coating like E30 may be appropriate. However, if the coating is at risk of coming in contact with hard objects, then a hard coating like E0 may be appropriate to resist scratches. If an application requires good corrosion protection and reasonably high hardness, then a coating like E10 or E20 may be appropriate.

This study supports the viability of CGE as a possible bio-based substitute for TMPGE. However, further work may be worthwhile to obtain a fuller understanding of CGE's benefits. Conducting EIS testing in different electrolytes would help to simulate performance in other environments. Other work could involve incorporating a zinc-rich pigment into the epoxy coating formulation to provide additional corrosion protection. Zinc is a more chemically active metal than iron is, so if a defect develops in the coating, the zinc in the pigment could corrode preferentially to the steel protected by the coating. This action would reduce the corrosion of the steel. Cost considerations of substituting TMPGE with CGE should also be analyzed to determine the economic factors involved.

6.3 Conclusions

Several conclusions can be drawn from this study. The first conclusion is that substituting CGE for TMPGE as the reactive diluent in epoxy coatings improved corrosion protection. This is evidenced by the relatively large R_p values for coatings formulated with CGE when compared with the control that was formulated with only TMPGE. The second conclusion is that substituting CGE for TMPGE had a negative impact on epoxy coating hardness. The third conclusion is that substituting CGE for TMPGE had no measurable effect on epoxy coating adhesion, flexibility, and impact resistance. Any of the four tested coatings may be attractive depending on the desired application. Further investigation regarding

performance in other environments and regarding the incorporation of a zinc-rich pigment could be beneficial future steps.

7 Literature Cited

1. "Economic Impact." *Economic Impact*, NACE International, impact.nace.org/economic-impact.aspx.
2. Jones, Denny A. *Principles and Prevention of Corrosion*. 2nd ed., Prentice Hall, 1996.
3. "Clean Air Act Standards and Guidelines for Petroleum Refineries and Distribution Industry." *Environmental Protection Agency*, United States Environmental Protection Agency, 13 Sept. 2018, www.epa.gov/stationary-sources-air-pollution/clean-air-act-standards-and-guidelines-petroleum-refineries-and.
4. Wicks, Zeno W., et al. *Organic Coatings: Science and Technology*. 3rd ed., John Wiley & Sons, Inc., 2007.
5. "Bisphenol A." *Sigma-Aldrich*, Sigma-Aldrich, www.sigmaaldrich.com/catalog/product/aldrich/239658?lang=en®ion=US.
6. "Practical Guide to Wetting Agents and Surface Modifiers." *Practical Guide to Wetting Agents and Surface Modifiers*, BASF, www.dispersions-pigments.basf.com/portal/load/fid830449/Wetting%20Agents%20and%20Surface%20Modifiers.pdf.
7. "Trimethylolpropane Triglycidyl Ether." *Sigma-Aldrich*, Sigma-Aldrich, https://www.sigmaaldrich.com/catalog/product/aldrich/430269?lang=en&region=US.
8. Wang, H., & Zhou, Q. Synthesis of Cardanol-based Polyols via Thiol-ene/thiol-epoxy Dual Click- reactions and Thermosetting Polyurethanes Therefrom. *ACS Sustainable Chemistry & Engineering* **2018** *6* (9), 12088-12095.
9. ASTM D3359-17, Standard Test Methods for Rating Adhesion by Tape Test, ASTM International, West Conshohocken, PA, 2017, www.astm.org

10. ASTM D4366-16, Standard Test Methods for Hardness of Organic Coatings by Pendulum Damping Tests, ASTM International, West Conshohocken, PA, 2016, www.astm.org
11. ASTM D3363-05, Standard Test Method for Film Hardness by Pencil Test, ASTM International, West Conshohocken, PA, 2005, www.astm.org
12. ASTM D522/D522M-17, Standard Test Methods for Mandrel Bend Test of Attached Organic Coatings, ASTM International, West Conshohocken, PA, 2017, www.astm.org
13. "Constant Phase Element." *Basics of EIS: Electrochemical Research-Impedance*, Gamry Instruments, www.gamry.com/Framework%20Help/HTML5%20-%20Tripane%20-%20Audience%20A/Content/EIS/Theory/Physical%20Electrochemistry%20and%20Circuit%20Elements/Constant%20Phase%20Element.htm.
14. "Gamry Echem Analyst." *Gamry Instruments*, Gamry Instruments, https://www.gamry.com.

8 Acknowledgments

A special thanks is in order for Dr. Qixin Zhou and Haoran Wang for supervising this project and for providing input and advice when necessary. I also wish to thank Dr. Zhou's research group for the materials and equipment necessary for completing the research. Finally, I wish to thank Dr. David Bastidas and Dr. Rajeev Gupta for acting as readers for this report and Dr. Hongbo Cong for his role as my Honors Advisor.